Mineralogical Magazine (2021), **85**, 49–67
doi:10.1180/mgm.2021.8

CAMBRIDGE
UNIVERSITY PRESS

Article - Frank Reith memorial issue

Biogeochemical formation of metalliferous laminations in surficial environments

Anicia Henne[1,2]*, Dave Craw[3], Jessica Hamilton[4], Anat Paz[1], Gemma Kerr[3], David Paterson[4], Jeremiah Shuster[5,6] and Gordon Southam[1]

[1]School of Earth and Environmental Sciences, The University of Queensland, St Lucia QLD 4072 Australia; [2]CSIRO Mineral Resources, Australian Resources Research Centre (ARRC), 26 Dick Perry Avenue, Kensington, WA 6151, Australia; [3]Geology Department, University of Otago, PO Box 56, Dunedin 9054, New Zealand; [4]Australian Synchrotron, ANSTO, Clayton VIC 3168 Australia; [5]School of Biological Sciences, The University of Adelaide, South Australia 5005, Australia; and [6]CSIRO Land and Water, Environmental Contaminant Mitigation and Technologies, PMB2, Glen Osmond, South Australia 5064, Australia

Abstract

Finely laminated (cm–µm scale) metalliferous precipitates are widespread in the surficial environment, especially around mineral deposits and reflect biogeochemical processes that can pervade near-surface environments on a larger scale. Examples in this paper involve precipitates of the transition metals Fe, Cu and Mn with minor Co, Ni, V and Zn; the metalloids As and Sb; and authigenic Au. Mobility and re-precipitation are driven primarily by geochemical disequilibrium, especially with respect to pH and redox states, that arises from complex interactions between biological processes, geological processes, and variations in the surrounding environment. Different degrees of chemical disequilibrium arise on small spatial scales on time scales of days to millennia. Interactions between biota, waters and rocks in these small near-surface settings affect the biogeochemical environments. Sulfur- and iron-oxidising bacteria are common biogeochemical agents associated with sulfide-bearing lithologies, but localised reductive environments can also develop, leading to gradients in pH and redox state and differential metal mobility. In general, there is commonly a spatial separation of Fe-rich precipitates from those with Cu and Mn, and other transition metals also follow Cu and Mn rather than Fe. Metalloids As and Sb have a strong affinity for Fe under oxidising conditions, but not under more reducing conditions. However, complex biogeochemical parageneses of laminated metalliferous deposits preclude prediction of finer formation details. The textures, mineral species, and metal associations within these deposits are likely to be encountered in all facets of mineral deposit development: initial exploration activity of near-surface locations, mining of shallow portions of orebodies, especially supergene zones, and downstream environmental management with respect to discharging metalliferous waters.

Keywords: metals, bacteria, biofilm, disequilibrium, groundwater, precipitation

(Received 28 October 2020; accepted 24 January 2021; Accepted Manuscript published online: 28 January 2021; Guest Associate Editor: Janice Kenney)

Introduction

Numerous aqueous environments around metal deposits host fine-scale (cm–µm) laminated metalliferous precipitates, especially in surficial environments, such as surface streams and groundwater. These laminated deposits constitute a record of the fluctuating redox conditions during their formation, which are due to their ephemeral nature and their fluctuations in composition and volume depending on weather events, seasonal variations and/or climate changes (e.g. Shuster *et al.*, 2018). Biological processes can affect metal-bearing geochemical systems and therefore add to the compositional variability of laminated deposits. Common examples include iron- and sulfur-oxidising bacteria that can catalyse acid-generating geochemical processes (Shuster *et al.*, 2018), photosynthesising organisms, whose activity can lead to diurnal and seasonal geochemical effects, the effects of temperature fluctuations on metabolism (Alpers *et al.*, 2003; Pope *et al.*, 2003; Andrade *et al.*, 2010) and biomineralisation (Heim, 2011). Consequently, most surficial environments are complex and dynamic biogeochemical systems in which biogenic and geogenic processes control mobilisation and re-precipitation of metals (Reith *et al.*, 2012*a*, 2015, 2020).

Biological activity in these environments, particularly that of bacteria, is especially important for mobilising and re-precipitation of metals around mineral deposits (Reith *et al.*, 2006, 2012a,b, 2013, 2015, 2020; Wakelin *et al.*, 2012a,b; Sanyal *et al.*, 2019). Understanding the biologically related processes causing mobility of metals in the surficial environment is important for quantifying environmental issues in the short term (human time scales; Warren and Haack, 2001; Gadd, 2007, 2010; Shuster *et al.*, 2018). Long-term (geological time scales) biologically mediated metal mobility is also of interest for geochemical exploration of mineral deposits (Reith *et al.*, 2012*a*, 2015; Wakelin *et al.*, 2012b). In addition, the precipitates from long-term biologically

***Author for correspondence:** Anicia Henne, Email: anicia.henne@csiro.au
This paper is part of a thematic set in memory of Frank Reith.
Cite this article: Henne A., Craw D., Hamilton J., Paz A., Kerr G., Paterson D., Shuster J. and Southam G. (2021) Biogeochemical formation of metalliferous laminations in surficial environments. *Mineralogical Magazine* **85**, 49–67. https://doi.org/10.1180/mgm.2021.8

© The Author(s), 2021. Published by Cambridge University Press on behalf of The Mineralogical Society of Great Britain and Ireland

https://doi.org/10.1180/mgm.2021.8 Published online by Cambridge University Press

mediated metal mobility can be significant for mineral processing and resource economics, especially in settings such as supergene alteration (Nordstrom and Southam, 1997; Enders *et al.*, 2006; Reith *et al.*, 2007, 2013; Henne *et al.*, 2019a).

This study provides a mainly mineralogical and geochemical overview of some of the biogeochemical systems that have produced laminated metalliferous precipitates in a variety of aqueous environments, from surface streams to the deep ocean, to illustrate the wide variety of laminated deposits. All of our examples form a record of biogeochemical fluctuations over time and have either an inferred or demonstrated biogeochemical component. We document some of the metalliferous similarities in this diverse selection of laminated deposits regardless of their contrasting parageneses, and also highlight some differences. The mineralogical and textural variations that we outline here attest to formation under fluctuating biogeochemical conditions in a complex interplay between biogenic and geogenic processes dominated by geochemical disequilibrium. The micro-scale layering related to varying degrees to biological activity in our examples emphasises the importance of understanding the biogeochemical processes within these microenvironments, and the important role that biogeochemical cycling of metals plays in the solubilisation and mineralisation of metals.

Study context and rationale

Laminated metal deposits through time

Eleven samples were selected (Table 1) that cover a broad range of metalliferous settings and metal combinations. These examples are presented in general order of age, from laboratory experiments (months), through historic mine sites (decades), to supergene weathering and deep-ocean processes (millions to tens of millions of years). Older deposits have fewer constraints on their formation processes and retain less evidence for biological activity. Hence, we combine that limited evidence with inferences from the younger examples to obtain an integrated view of the biogeochemical processes and their metallic residues through time.

Samples in this study were selected from material that we obtained in a range of previous studies for entirely different purposes, as outlined in the references in Table 1. These samples were collected from a wide variety of settings associated with mining, exploration and rehabilitation activities and include samples from historic mine waters in the South Island of New Zealand, acid mine drainage in California, USA, anthropogenically neutralised mine drainage in Queensland, Australia, along with samples from oxidised and supergene zones overlaying ore bodies in the South Island of New Zealand, in Salobo, Brazil and Queensland, Australia. In addition, one sample originated from a laterite/soil interface associated with plants over iron ore bodies in Serra Norte, Brazil and one from the North Pacific Ocean floor (manganese nodule). We also include a sample derived from long-term laboratory experiments designed to model the biogeochemical weathering of Cu-bearing lithologies at Salobo, Brazil. These samples, and the near-surface settings from which they were taken, were chosen because they display evidence of fluctuating biogeochemical conditions that have led to laminated deposits. The details of biological and geochemical contributions to formation of these laminated deposits are covered more specifically in references cited herein and other related studies, and some biological aspects of the geologically older material can only be inferred on the basis of the known near-surface settings.

Our chosen examples all show evidence for fluctuating biogeochemical conditions during their formation. We focus on the generalised variations and gradients in redox and pH conditions that have contributed to the formation of these disparate precipitates, and the mineralogical results of these processes. Most of these examples have dominant or primary metals (especially Fe and/or Mn), in which geochemical variations largely control the precipitation processes. These dominant metals are accompanied by other metals that become incorporated into laminated precipitates as a result of secondary or collateral effects.

Theoretical basis for biogeochemical variations

Although biological processes can catalyse chemical reactions that operate within thermodynamic principles, there is an underlying thermodynamic control on the formation of laminated metallic deposits. In the surficial environment, the Gibbs free energy change of a reaction, $\Delta G_{\text{reaction}}$, has two components, the standard Gibbs free energy of the reaction, $\Delta G^{\circ}_{\text{reaction}}$, and the reaction quotient, Q:

$$\Delta G_{\text{reaction}} = \Delta G^{\circ}_{\text{reaction}} + RT \ln Q \quad (1)$$

where R is the gas constant and T is the temperature (~298 K was chosen as an average temperature for the surficial environments modelled in this study). The reaction quotient Q is the ratio of multiplied activities of reaction products and multiplied activities of reactants. At equilibrium, Q is equal to the equilibrium constant, K_{eq}. As $\Delta G_{\text{reaction}}$ is zero at equilibrium,

$$\Delta G^{\circ}_{\text{reaction}} = -RT \ln K_{\text{eq}} \quad (2)$$

Combining reactions 1 and 2 yields:

$$\Delta G_{\text{reaction}} = RT(\ln Q - ln K_{\text{eq}}) \quad (3)$$

Hence, when $Q < K_{\text{eq}}$ the reaction goes forward, and when $Q > K_{\text{eq}}$ the reaction is reversed. The special condition of equilibrium is relatively rare in dynamic surficial environments. Bacteria, in particular, can use enzymes to gain energy for metabolic processes that catalyse reactions from a disequilibrium state where $Q < K_{\text{eq}}$ and thereby can accelerate the rate at which reactions progress towards equilibrium ($Q = K_{\text{eq}}$) (Deamer and Weber, 2010).

As an example, one of the most common reactions in the surficial environment is the relationship between dissolved ferrous iron and ferrihydrite:

$$Fe^{2+} + 0.25O_2 + 2.5H_2O \rightarrow Fe(OH)_3 + 2H^+ \quad (4)$$

The reaction quotient is:

$$Q_{\text{ferrihydrite}} = [H^+]^2/([Fe^{2+}](pO_2)^{0.25}) \quad (5)$$

where pO_2 is the partial pressure of oxygen. Therefore, the ferrihydrite reaction (4) is dependent on pH, oxygen partial pressure or redox conditions, and the amount of dissolved ferrous iron. While temperature can be an important variable within surficial environments, here we focus on fluctuations of the three variables above, as they are common in surficial environments for a wide range of biogeochemical reasons, as outlined below. Consequently, disequilibrium dissolution and/or precipitation of iron (and other metals) is a widespread biogeochemical phenomenon, as in many of the examples in Table 1 that are described below.

https://doi.org/10.1180/mgm.2021.8 Published online by Cambridge University Press

https://doi.org/10.1180/mgm.2021.8 Published online by Cambridge University Press

Table 1. Summary of examples of laminated metal deposition from a range of aqueous environments over a range of time scales.

Material	Locality	Biota	Metals	Setting	pH	Climate	Time, yrs	Figs	Refs
Ferrihydrite precipitates	Laboratory experiments on Salobo IOCG rocks	IOB *Acidithiobacillus ferrooxidans*	Fe, Cu	Leaching of Fe-rich rocks	3–6	Controlled, wet, 30°C	0.1–1	1	1
Ferrihydrite weathering cements	Macraes orogenic gold mine, New Zealand	SOB, IOB*	Fe, As, Hg.	Mine tailings	2–5	Temperate-semiarid	10 to 100	2	2
As-rich weathering cements	Waiuta orogenic gold mine, New Zealand	IOB, SRB, organic decay fungi*	As, Fe	As-rich mine tailings	3–6	Wet temperate	10 to 100	2	3
Underground tunnel precipitates	Iron Mountain mine, California, USA	IOB, SOB*	Fe, Cu, Zn	Acid mine drainage	−1 to 3	Seasonal wet/dry	10 to 100	2	4
Discharge stream precipitates	Mt Chalmers mine Queensland, Australia	Moss, algae microinvertebrates	Cu, Zn	Treated acid mine drainage	6–7	Subtropical, seasonal wet/dry	10 to 100	3	5
Oxidised stibnite, pyrite, arsenopyrite	Orogenic Au-Sb deposit, New Zealand	IOB, SOB, SRB*	Sb, As, Fe	Oxidation zone	6–8	Cool temperate	10^3 to 10^4	4	6
Gold particles, saprolite and paleoplacers	Otago Schist, New Zealand	IOB, SOB, SRB*	Au, Ag	Supergene zone	7–8	Cool temperate-semiarid	10^6 to 10^7	9	7
Veins in lateritic saprolite	Salobo IOCG mine, Brazil	IOB, MOB, SOB	Cu, Mn, Ti, V	Supergene zone	5–8	Subtropical, seasonal wet/dry	10^6 to 10^7	5,6	8
Manganese nodule	North Pacific Ocean	MOB, Mn-oxidising Archaea*	Mn, Cu, Fe, Co, Ni, Ti, Zn	Deep ocean floor	8	Saline, <5°C	10^6 to 10^7	10	9
Fe-oxide precipitates in plant root cavity	Vale N1 mine (Serra Norte), Brazil	Cyperaceae (sedge), IOB, IRB	Fe	Laterite regolith	7–8	Subtropical, seasonal wet/dry	10^6 to 10^7	8	10
Native copper from saprolite	Mt Isa, Australia	IOB, SOB*	Cu, Fe, As	Supergene zone	6–8	Currently arid-monsoonal	10^7 to 10^8	6,7	11

IOB = Fe-oxidising bacteria; IRB = Fe-reducing bacteria; SOB = S-oxidising bacteria; SRB = S-reducing bacteria; MOB= Mn-oxidising bacteria; *Inferred. General references: 1. Henne *et al.* (2019a); 2. Kerr and Craw (2020); 3. Kerr *et al.* (2018); 4. Alpers *et al.* (2003); 5. Henne *et al.* (2021); 6. Craw and Kerr (2017); 7. Reith *et al.* (2012b); Craw *et al.* (2015); Craw and Lilly (2016); 8. Henne *et al.* (2019a, 2020); 9. Manceau *et al.* (2014); Shiraishi *et al.* (2016); 10. Levett *et al.* (2020); Paz *et al.* (2020); 11. Salama *et al.* (2016).

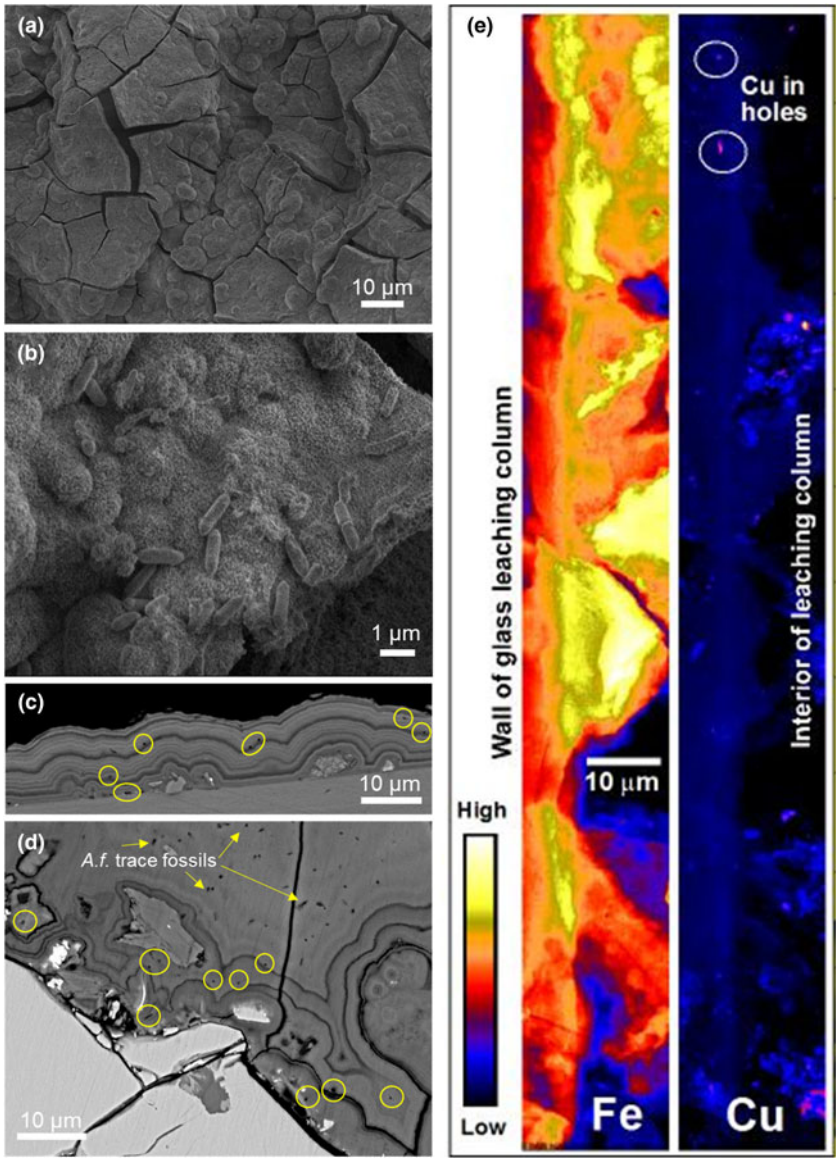

Fig. 1. Laminated precipitates formed in laboratory-based biogeochemical weathering experiments. (a) General SEM view of ferrihydrite precipitate with dehydration cracks from sample preparation on a rock clast. (b) Cells of *A. ferrooxidans* on ferrihydrite precipitate. (c) Back-scattered electron image of a section through ferrihydrite precipitate coating the wall of a leaching column with trace fossils of *A. ferrooxidans* (yellow circles). (d) Back-scattered electron image of a section through laminated ferrihydrite precipitate with trace fossils of *A. ferrooxidans* (yellow circles and arrows) on a chalcopyrite clast. (e) XFM element-distribution maps for Fe and Cu of laminated ferrihydrite precipitate on the wall of the experimental vessel. Enhanced Cu deposition at bacterial trace fossils are indicated (white circles).

Methods

Mineralogy and textures for most samples have been characterised using polished thin sections, light microscopy, X-ray diffraction (XRD) and synchrotron X-ray fluorescence microscopy (XFM). More detailed textural and geochemical observations were made using scanning electron microscopy (SEM) with energy dispersive X-ray spectroscopy (EDS) on polished thin sections and freshly-broken surfaces. Details regarding SEM instrument parameters and settings are given in Kerr *et al.*, (2018) and Henne *et al.*, (2019a, 2020).

Synchrotron X-ray fluorescence microscopy was used on selected samples to obtain relative element-distribution maps of transition metals, with detection limits of ~100 ppm. The XFM maps were generated on the XFM beamline (Paterson *et al.*, 2011) at the Australian Synchrotron, ANSTO. The maps were generated using a monochromatic X-ray beam at 18,500 eV, focussed using Kirkpatrick–Baez mirrors to ~2 µm with a dwell per pixel of 0.2 to 0.5 msec. Data were collected with a Maia detector (Ryan *et al.*, 2010, 2014), and full spectrum data (sensitive to elements from Sr to Zr) were analysed using the *GeoPIXE* software program (Ryan, 1999). X-ray fluorescence microscopy element data are derived from irradiation of the entire thickness (~30 µm) of the polished section, so the technique cannot resolve sub-µm particles amongst underlying and/or overlapping particles.

In addition, the X-ray absorption near edge spectroscopy (XANES) mapping capability of the XFM beamline was used to investigate Cu speciation within regions of interest that were selected from element-distribution maps of selected samples. Copper *K*-edge XANES analysis was undertaken over the energy range of 8900 to 9300 eV, with maximum energy steps of 25 eV in the post-edge region (9100 to 9300 eV), and minimum energy steps of 0.5 eV over the edge (8976 to 9000 eV). Spectra were collected across regions of interest with a step size of 4–5 µm. Dwell times varied between samples within the range of 0.5 to 5 msec per pixel. The reference materials used as standards for comparison were native copper tape, Cu(I) chloride, Cu(I) oxide, Cu(II) chloride, Cu(II) oxide, Cu(II) carbonate and Cu(II) sulfate. *GeoPIXE* was used to process the data before *Athena* software was used for background subtraction and normalisation (Ravel and Newville, 2005).

https://doi.org/10.1180/mgm.2021.8 Published online by Cambridge University Press

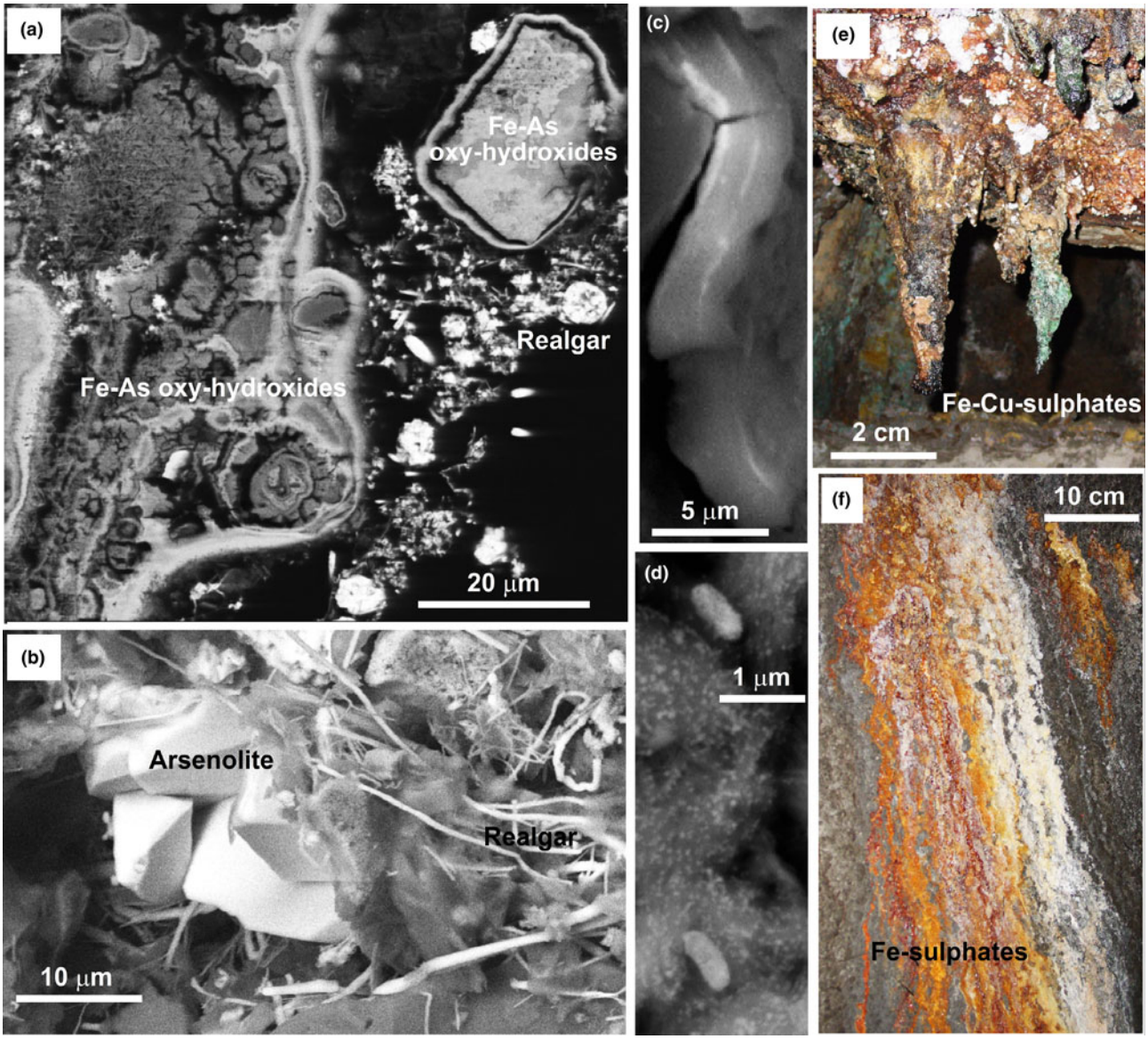

Fig. 2. Laminated precipitates formed at historic mines. (a) SEM view of cemented tailings on a wood fragment; Waiuta orogenic gold mine, New Zealand. Laminated As-bearing Fe-oxyhydroxide precipitates (mid-grey) coat some of the clasts, with an outer layer of realgar (AsS; bright white) precipitate. (b) Magnified view of the same deposit as in (a), showing arsenolite crystals (As_2O_3) with overgrowths of hair-like realgar. (c) SEM view of As–Hg-bearing ferrihydrite cement in historic tailings from Macraes orogenic gold mine, New Zealand, in which Hg was used for gold extraction. The cement is laminated with differing proportions of As and different Hg contents are shown as brighter and darker layers. (d) Magnified view of the same deposit as in (c), showing precipitate lamina rich in schuetteite ($Hg_3[SO_4]O_2$) and possibly preserved bacterial cells partially per-mineralised by schuetteite. Some of the smallest white dots are nanoparticulate liquid Hg droplets. (e) Photograph of laminated precipitates forming stalactites on the roof of an underground tunnel, Iron Mountain mine, California. (f) Photograph of laminated precipitates on the wall of the mine in (e).

Descriptions of laminated metalliferous deposits in different aqueous environments

Laminated precipitates in laboratory weathering experiments

In laboratory-scale weathering experiments of fresh rocks from the Salobo iron-oxide copper–gold (IOCG) deposit in Brazil, finely laminated metalliferous precipitates were produced within ~400 days in a biogeochemical system dominated by *Acidithiobacillus ferrooxidans*, an acidophilic, iron-oxidising bacterium (Henne *et al.*, 2018, 2019a, 2020). These experiments were conducted in small-scale (10 cm^3) polypropylene columns, partially filled with crushed, weakly mineralised rock. The rocks were dominated by iron-bearing silicates with minor disseminated chalcopyrite and bornite. A strain of *A. ferrooxidans* was cultured from the Salobo mine site and used for the experiments, as described by Henne *et al.* (2018, 2019a,b, 2020). Samples of the column solutions (2 mL) were obtained every two days and replaced with fresh growth medium to sustain active metabolic activity of bacteria. After completion of the experiments, some columns were opened to view the precipitates that had formed on rock clasts (Fig. 1a, b). Some columns were embedded *in situ*, sectioned, and polished for examination by light microscopy, SEM and XFM (Fig. 1c,d,e; Henne *et al.*, 2019a, 2020).

Secondary precipitates that formed around some particles and on the walls of the columns were dominated by ferrihydrite ($Fe[OH]_3$; although this material was largely amorphous). Some

https://doi.org/10.1180/mgm.2021.8 Published online by Cambridge University Press

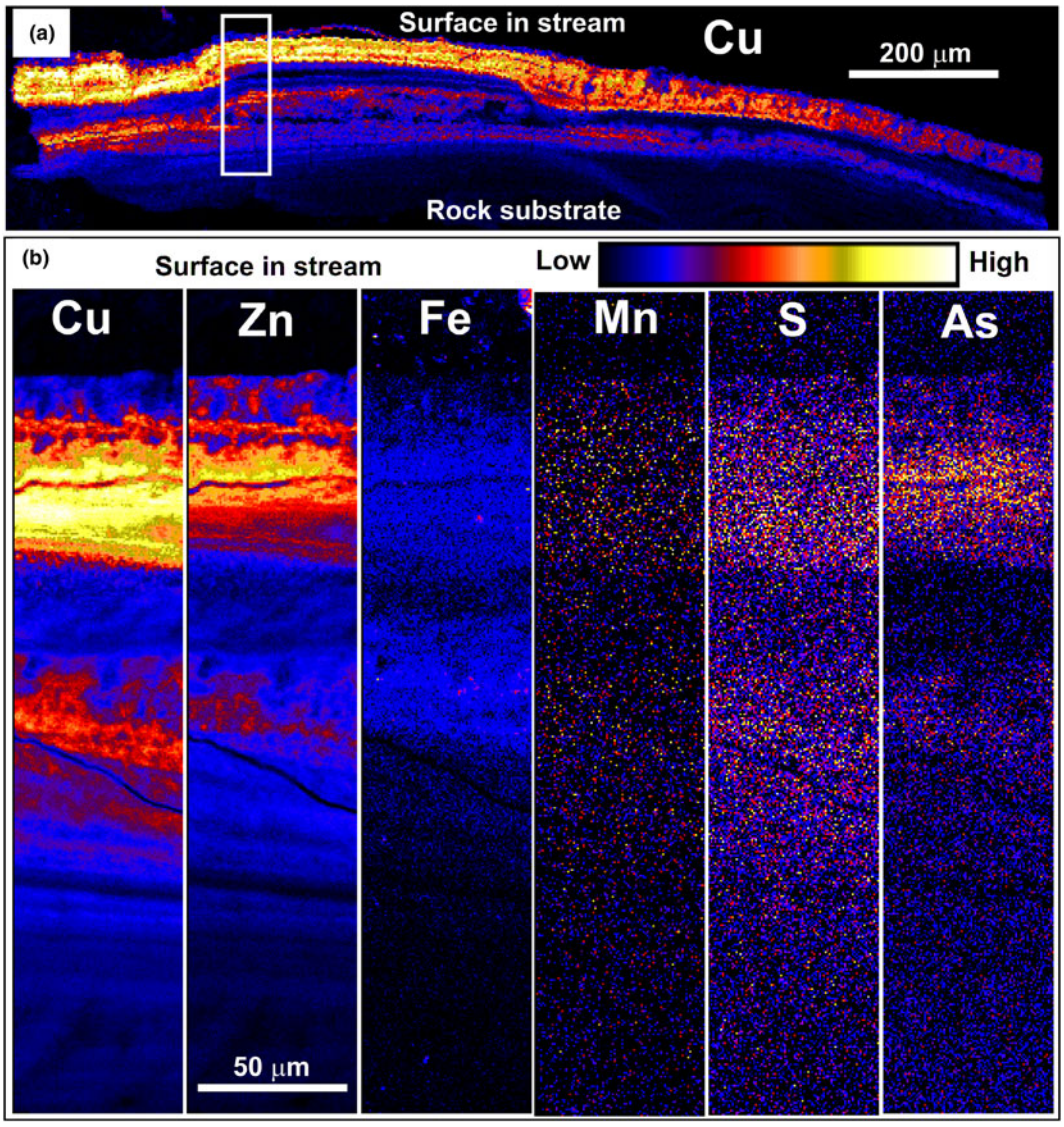

Fig. 3. XFM element-distribution maps of a thin section through laminated mineral precipitates on a biofilm growing on a cobble downstream of the treated AMD at the Mt Chalmers Cu–Au mine, Australia. (a) General view of Cu contents in the laminated deposit. (b) Magnified view of the portion indicated in (a), showing relative concentrations of Cu, Zn, Fe, Mn, S and As.

of the precipitates exhibited fine (micrometre-scale) laminations reflecting differing degrees of hydration, chemical composition, and different nanoparticulate particle sizes. These laminations followed the relief of the substrate as well as abundant micrometre-scale circular holes that were trace fossils of individual *A. ferrooxidans* cells, permineralised *in situ* during deposition of acicular ferrihydrite (Fig. 1c,d). In general, the distribution of Cu followed the deposition of ferrihydrite laminations, which contained up to 7 wt.% Cu. Interestingly, Cu content was elevated locally within bacterial trace fossils (Fig. 1e).

Laminated precipitates in historic mine wastes

Laminated precipitates found in historic mine wastes, which were abandoned without rehabilitation, provide an opportunity to observe results of biogeochemical processes over human time scales. These laminations record changes in biogeochemical conditions during surficial weathering processes, which influence metal mobility. In two examples from orogenic gold deposits in New Zealand (Waiuta mine and Macraes mine; Fig. 2a–d; Table 1), metals have been dissolved and redeposited by shallow groundwater, forming precipitates that cement the waste materials (Fig. 2a–d). These cementation processes are affected by the weather and seasonal variations that are imposed on inhomogeneous materials that will inevitably include biological components. The constantly changing groundwater compositions result in laminated precipitates reflecting this wide range of biogeochemical conditions. The ore, and subsequent tailings, from these mines contained abundant arsenic (As). The ambient pH at both sites was circumneutral because of ample carbonate in the rocks, but processing of the ore and subsequent weathering has resulted in localised acidification within the tailings deposits (Table 1).

Tailings from the Waiuta mine have been cemented variably by As minerals with a wide range of oxidation states, and these different minerals occur in close proximity at the micrometre-scale (Fig. 2a,b). These tailings were deposited in a shallow (~10 m) depression that has been water-saturated for >80 years and subjected to regular heavy rain events in a wet climate (rainfall >2000 mm/year). The

https://doi.org/10.1180/mgm.2021.8 Published online by Cambridge University Press

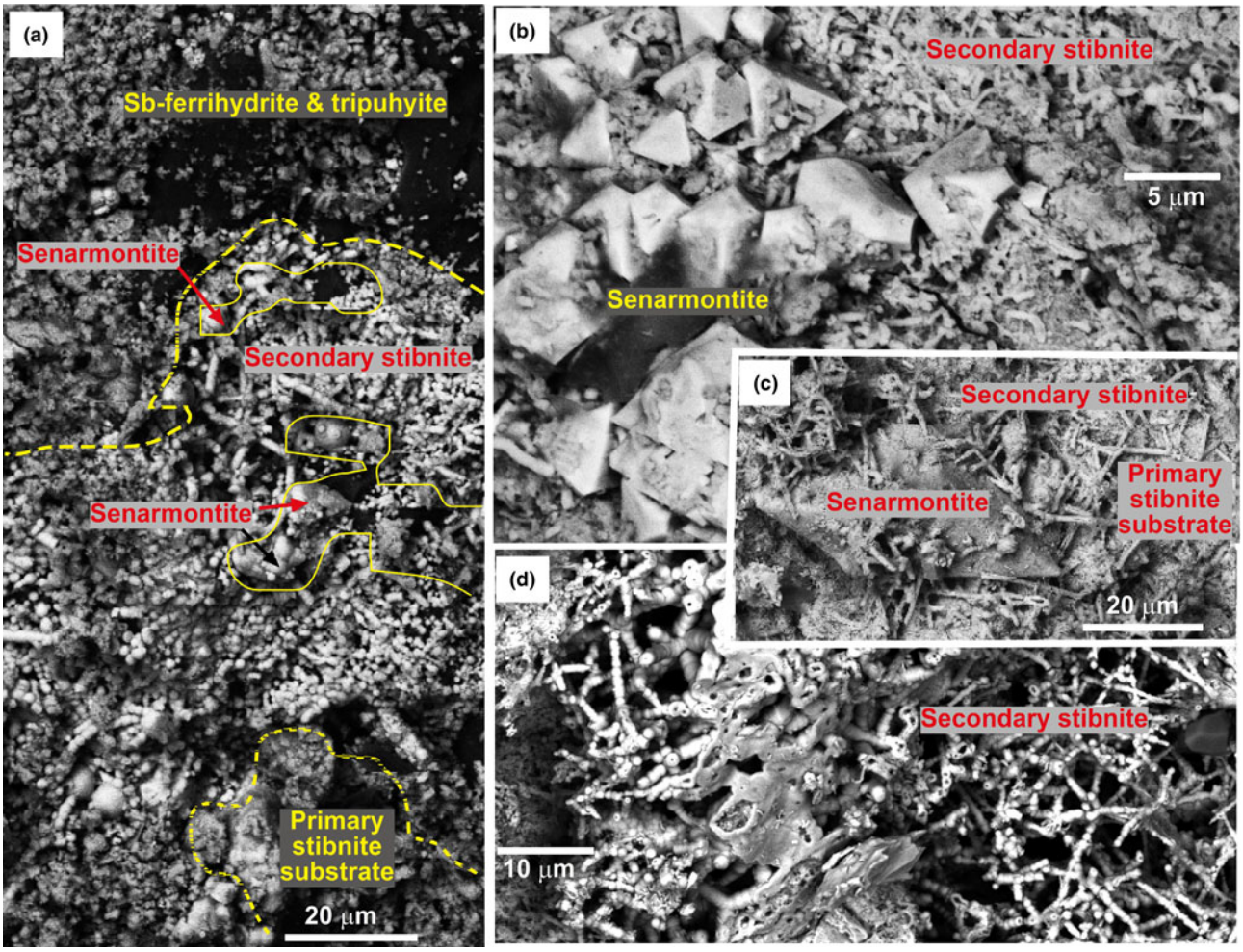

Fig. 4. SEM images of laminated secondary Sb minerals developed in an oxidised Au–As–Sb orogenic deposit, Otago Schist, New Zealand. (a) General view of contrasting redox minerals developed on primary stibnite (bottom), with secondary stibnite beneath Sb-bearing ferrihydrite and tripuhyite ($FeAsO_4$). (b, c) Magnified view of secondary minerals in the redox gradient in (a), with secondary stibnite overgrowing secondary senarmontite crystals (Sb_2O_3). (d) Magnified view of secondary stibnite, showing a tubular morphology produced potentially by filamentous bacteria.

deposit hosts abundant organic matter, including mosses, algae and bacteria, and some woody material from the surrounding rainforest (Kerr *et al.*, 2018). The most chemically-reduced cementing mineral, realgar, occurred principally on decomposing wood fragments within the tailings (Fig. 2a,b). This setting has resulted in extreme and fluctuating biogeochemical redox gradients within the tailings, leading to laminated precipitates that range from highly oxidised to highly reduced (Fig. 2a,b).

In contrast, the historic tailings from the Macraes mine have been weathering in a semiarid climate (rainfall ~600 mm/year) for ~80 years with associated evaporation facilitating formation of dry, hard, As-bearing ferrihydrite cement (Fig. 2c,d). Carbonaceous debris and relict sulfide minerals within the tailings have facilitated formation of small scale (micrometre to millimetre) redox gradients within the thin (<1 m) cemented deposit that is fully exposed to seasonal weather variations ranging from hot summers (>30°C days) to cold winters (<10°C nights). Historically, mercury amalgamation was used for gold extraction, and some remnants of this Hg remain in the tailings as liquid Hg droplets and as the more oxidised mineral schuetteite (Fig. 2c,d). Mercury has been incorporated variably into the ferrihydrite cement, forming distinct laminations (Fig. 2c,d). Liquid mercury droplets coexist with, and have locally formed on, schuetteite precipitates, and *vice versa* (Fig. 2d), reflecting the variable and fluctuating redox gradients in the tailings. Partially permineralised bacterial cells (Fig. 2d) attest to a biological component of the cementation processes.

Laminated precipitates from acid mine drainage

Aqueous environments affected by acid mine drainage (AMD) commonly host laminated deposits (Shuster *et al.*, 2017, 2018). Acid mine drainage results from discharge of shallow groundwater that has been affected by oxidation of sulfide minerals (especially pyrite) that have been exposed by mine excavations. From a biogeochemical perspective, sulfide oxidation is facilitated invariably by a wide range of bacterial species involving various reactions (Baker and Banfield, 2003; Johnson and Hallberg, 2005; Dold, 2014; Quatrani and Johnson, 2018). The historic Iron Mountain underground mine in California, USA (Fig. 2e,f; Table 1) is one of the most spectacular examples of AMD in the world where laminated metalliferous precipitates have formed. At the Iron Mountain underground mine, bacterially mediated oxidation reactions generated underground waters with a pH that ranges down to negative values (Alpers *et al.*, 2003). The resulting AMD compositions

https://doi.org/10.1180/mgm.2021.8 Published online by Cambridge University Press

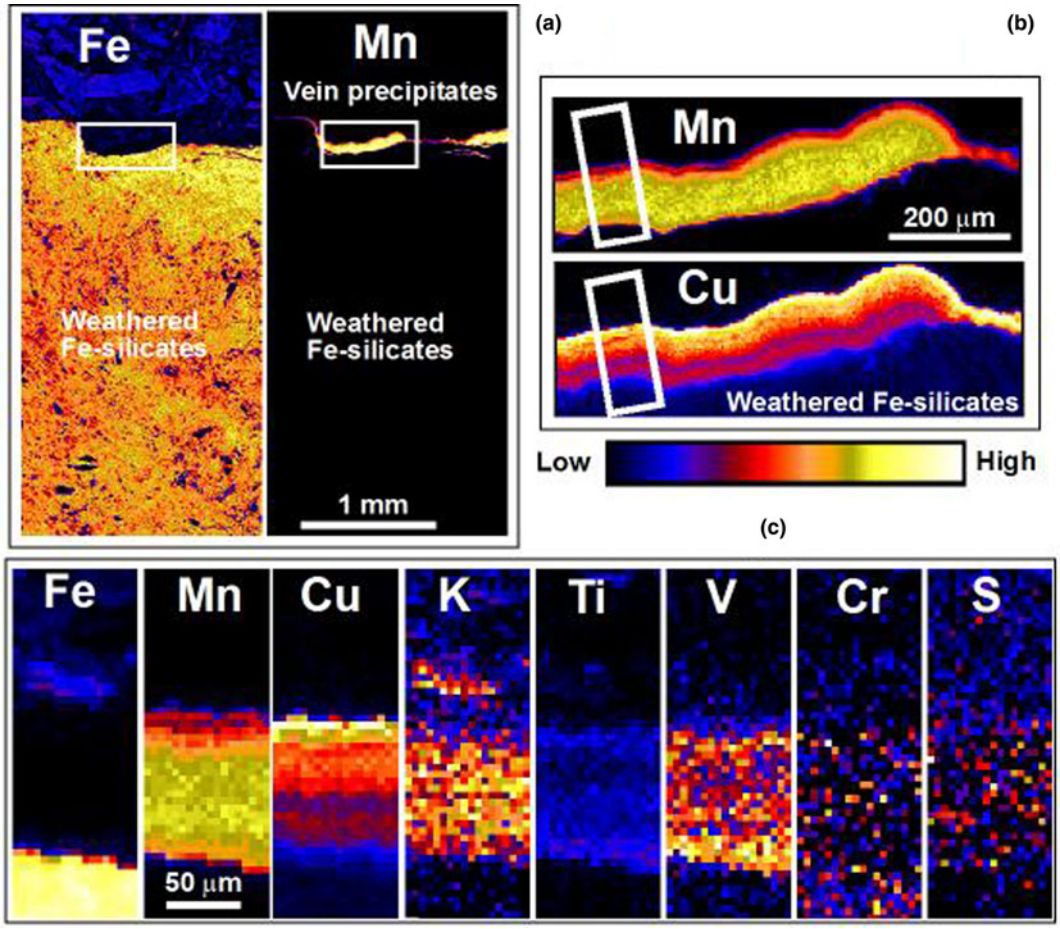

Fig. 5. XFM element-distribution maps of a thin section through a laminated vein formed during weathering of the Salobo IOCG deposit, Brazil. (a) Fe and Mn maps show the location of the vein (Mn rich) on the margin of oxidised rock (Fe rich). (b) Magnified view of the vein (as indicated in (a) showing laminae enriched in Mn and Cu. (c) Juxtaposed elemental sections through the vein, as indicated in (b).

change on time scales of seasons to years (Alpers *et al.*, 2003) and precipitates are laminated accordingly (Fig. 2e,f). Most of the precipitates are dominated by ferrous and ferric sulfate minerals (Fig. 2e,f), reflecting the very high dissolved sulfate concentrations in the AMD and fluctuating redox conditions (Alpers *et al.*, 2003). In addition, variable amounts of Cu and Zn sulfate minerals contributed to the laminated precipitates (Fig. 2e).

In an example of pH neutral surface waters at the Cu–Au mine at Mt Chalmers, Queensland, Australia (Table 1), AMD derived from tailings and relict mine walls have been neutralised with alkaline waste rock. Treatment of AMD discharges from historic mines is becoming common practice at many sites to ameliorate the downstream environmental effects. Treatment typically involves raising the pH using an acid-consuming material. The neutralisation of discharging waters at Mt Chalmers, which initially had a low pH (<4) and very high Cu and Zn concentrations, caused Cu and Zn sulfate precipitation on downstream cobbles. Precipitates are locally intergrown with biofilms, creating spectacularly laminated metalliferous deposits (Fig. 3a,b). The biofilms contain a wide variety of bacteria and archaea, some of which are photosynthetic, as well as moss, algae and macroinvertebrates. Some parts of the biofilms also include fossilised fragments of eukaryotes that have enhanced localised Cu and Zn deposition (Henne *et al.*, 2021).

Laminated precipitates from supergene weathering and oxidation

Laminated metalliferous precipitates, formed during incipient weathering of sulfide-bearing deposits, record the steep redox gradient between the primary sulfides and the most oxidised exterior minerals exposed to the atmosphere and/or oxygenated groundwater. Our example from an orogenic gold deposit from New Zealand (Table 1) of this type of redox gradient is on primary stibnite (Fig. 4a–d). The sulfides of the deposit have been exposed at the surface by erosion on a steep mountainside, and a thin (<1 m) zone of variably oxidised metallic secondary minerals has formed, with minimal metal mobility as transformations occurred largely *in situ*. The secondary minerals have a complex paragenesis of mutual overgrowths in crude layering within the redox gradient (Fig. 4a–d). The most oxidised veneer consists of Sb-bearing ferrihydrite and tripuhyite, and variably distributed senarmontite and secondary stibnite have formed in between the oxidised veneer and the primary stibnite (Fig. 4a). The senarmontite locally overgrows secondary stibnite and is locally overgrown by the secondary stibnite (Fig 4b–d). The secondary stibnite has a distinctive tubular texture with a high surface area reminiscent of permineralised filamentous bacteria, indicating a biological influence on formation (Fig. 4d).

https://doi.org/10.1180/mgm.2021.8 Published online by Cambridge University Press

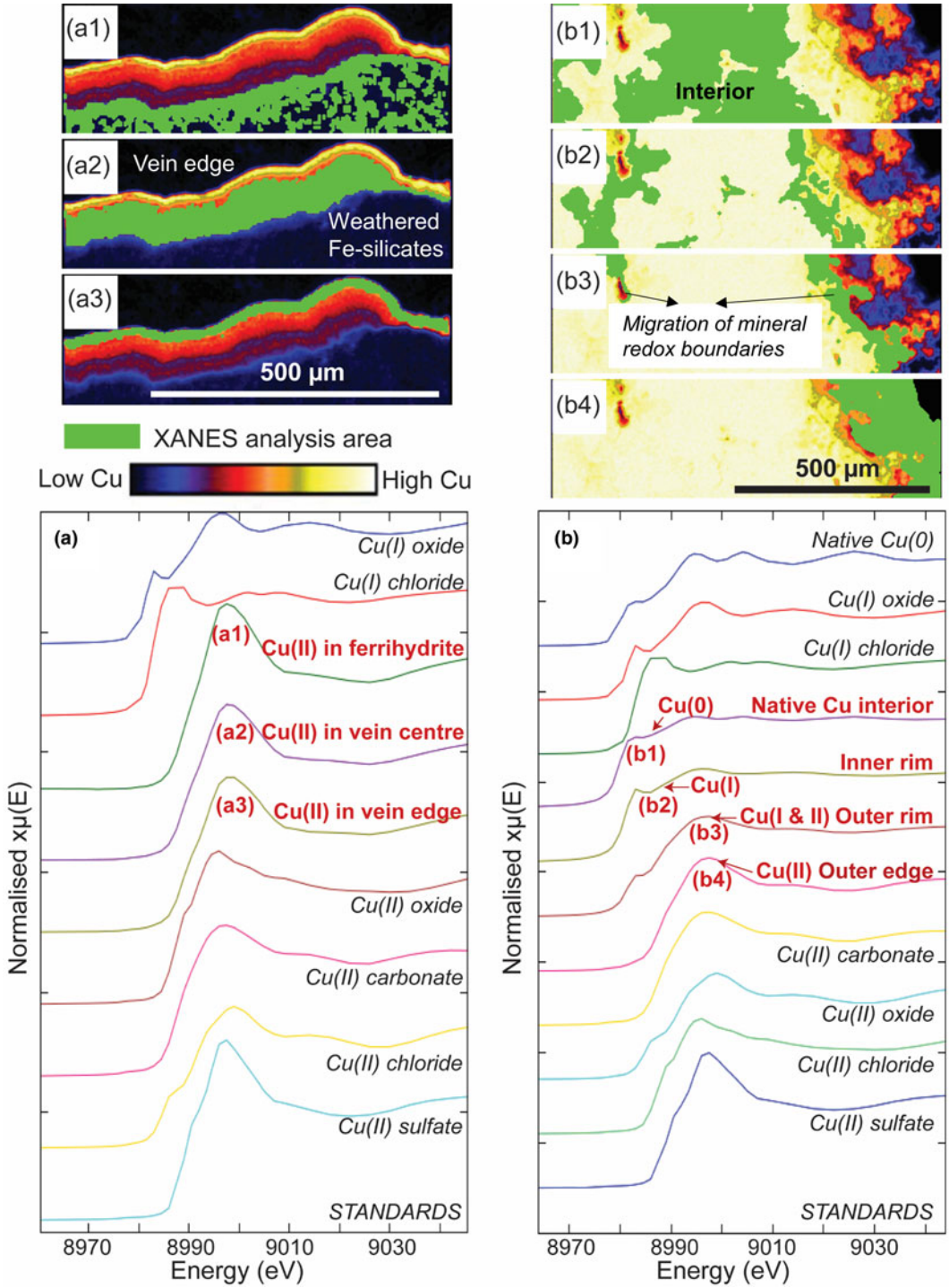

Fig. 6. Regions of interest from which Cu XANES spectra are extracted are numbered and highlighted in green, and are shown against a background map of Cu *K*-edge fluorescence intensity at 9.3 keV. A range of Cu(0), Cu(I) and Cu(II) standards are shown for comparison. (a) Spectra from the laminated vein and its substrate in saprolite from the Salobo mine (Fig. 5). (b) Spectra from the interior, inner and outer rim zones, and outer edge of the native copper sample from Mt Isa (Fig. 7).

More advanced weathering and oxidation was observed in our example from the saprolitic zone developed on the Precambrian Salobo IOCG deposit of Brazil (Fig. 5a–c; Table 1). This led to the development of a subsurface saprolitic zone in which the rocks have been oxidised extensively and variably altered to clays. This oxidation and alteration was driven partly by a wide range of bacteria, including Fe-, Mn- and S-oxidisers and Fe-reducers, that occur within water-saturated fractures exposed by the mine excavation (Henne *et al.*, 2020). In this saprolitic zone, typically more extensive metal mobility has occurred than in the previous incipient weathering example, and metal-bearing veins can form in structurally controlled sites. The example from the saprolitic zone developed at Salobo consists of a delicately laminated Cu- and Mn-rich vein that has formed on a fracture

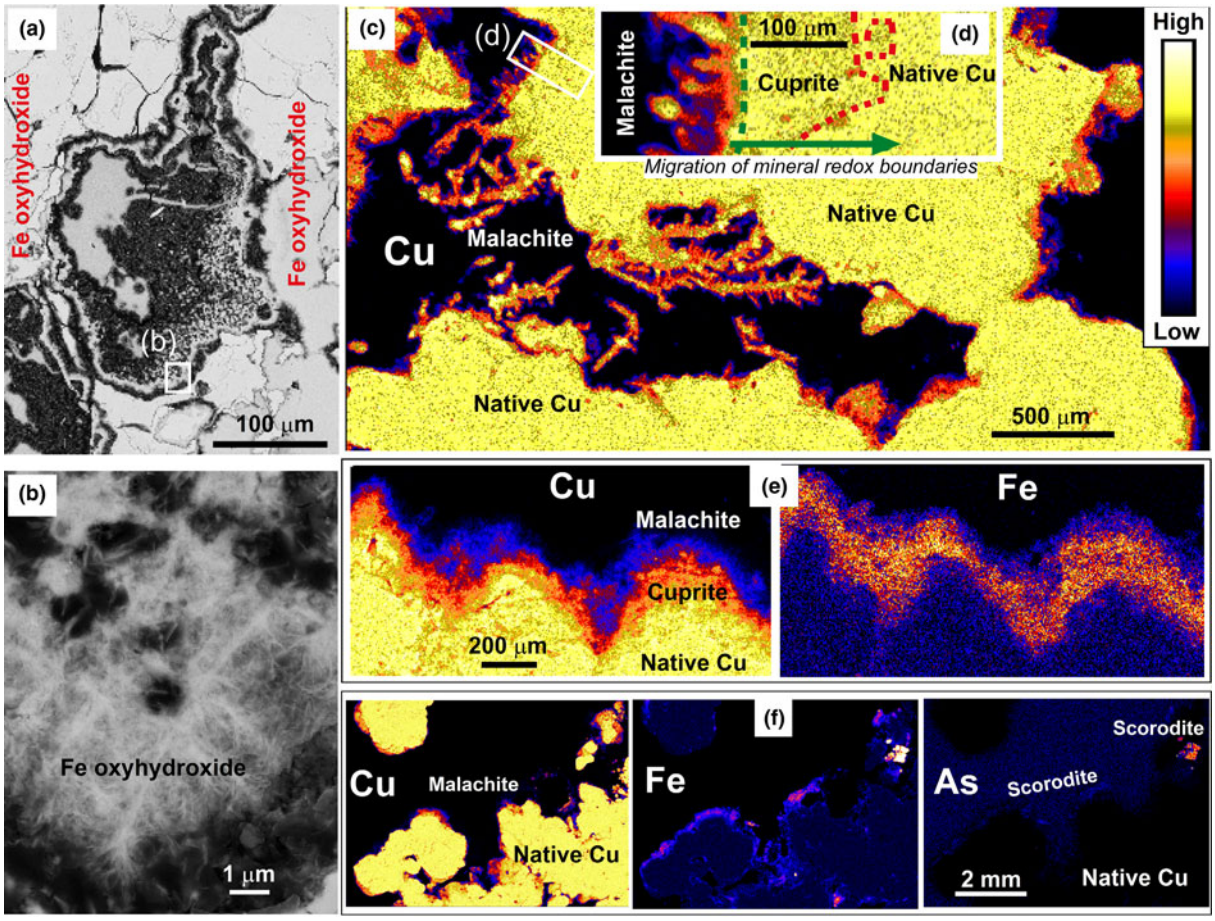

Fig. 7. SEM images and XFM element-distribution maps of laminations observed in supergene samples from Mt Isa, Queensland, Australia. (a) Back-scattered electron image of a cross-section through Fe-oxyhydroxides in native-copper-bearing rocks organised in colloform textures. (b) Potential bacteria fossil remnant in Fe-oxyhydroxide with acicular texture. (c) Copper XFM map of laminated rims on a supergene native copper nugget. (d) Magnified view of the rim zone in (a), showing principal minerals. (e) Paired Cu and Fe XFM maps of rim layers. (f) Copper, Fe and As XFM maps of rim layers. The As map has high background from the mounting glass, which obscures a zone of As enrichment that follows the outer edge.

surface in a rock dominated by weathered Fe-silicates (Fig. 5). Although there is abundant Fe in the general environment, there is only minor Fe in the vein (<1 wt.%; Fig. 5a,c). However, the vein includes a wide range of other elements in addition to the dominant Cu and Mn (Fig. 5c). Synchrotron-based XANES (Fig. 6a) revealed that Cu within the vein material, and the relatively low levels within the ferrihydrite substrate, occurred as Cu(II).

A common component of supergene weathering zones on copper-rich mineral deposits is native copper, which typically forms in the lower (more reduced) portions of an overall redox gradient in these zones. The example we depict in Fig. 7a–d is from the saprolitic weathering zone on the Precambrian rocks of the Mt Isa inlier in Queensland, Australia (Table 1). Weathering and progressive oxidation have resulted in the formation of a laminated rim zone around the mass of native copper (Fig. 7a–d). The redox gradient and associated mineralogy are similar to that of the supergene zone over the Salobo deposit in which we have abundant evidence for bacterial involvement (previously described above), and the Fe-oxyhydroxide minerals associated with native Cu grains in the Mt Isa samples display the acicular texture typical of Fe-oxyhydroxide precipitates facilitated by Fe-oxidising bacteria (Loiselle *et al.*, 2018) and bacterially sized moulds within these precipitates (Fig. 7a,b). The outermost part of the native copper rim zone consists of crystalline malachite (Fig. 7c–f) that is readily identifiable in hand specimen and is clearly a Cu(II) mineral in XANES analysis (Fig. 6b). The innermost portion of the rim zone shows up in incident light microscopy and XFM mapping as a diffuse zone that is different texturally from both the outermost crystals and the native Cu interior (Fig. 7d,e). This inner rim is shown by XANES analysis (Fig. 6b) to contain Cu(I) and is presumed to be cuprite. Iron is confined to the outer layers (Fig. 7e,f), and some relatively Fe-rich parts of this layer contain arsenic, possibly as scorodite (Fig. 7f).

At the interface of saprolitic rock and lateritic soil, more advanced oxidation during weathering and progressive leaching of mobile metals can leave a goethite-cemented zone known variously as ferricrete, duricrust, or canga (Gagen *et al.*, 2019; Levett *et al.*, 2020; Paz *et al.*, 2020). In our samples of canga over a supergene Fe deposit near the Serra Norte mine in Brazil (Table 1), deposits of Fe-oxyhydroxides dominated by goethite form a hard surface crust to the landscape. Native sedges (*Cyperaceae*) grow in rupestrian grasslands on the canga and extend their roots into the Fe-rich substrate (Fig. 8a). Biogeochemical processes have led to the formation of laminations with varying proportions of Fe-oxyhydroxides at a range of scales: around centimetre root channels (Fig. 8a,b), and in smaller root-related cavities (tens of μm; Fig. 8c). Microorganisms are preserved extensively as permineralised fossils

https://doi.org/10.1180/mgm.2021.8 Published online by Cambridge University Press

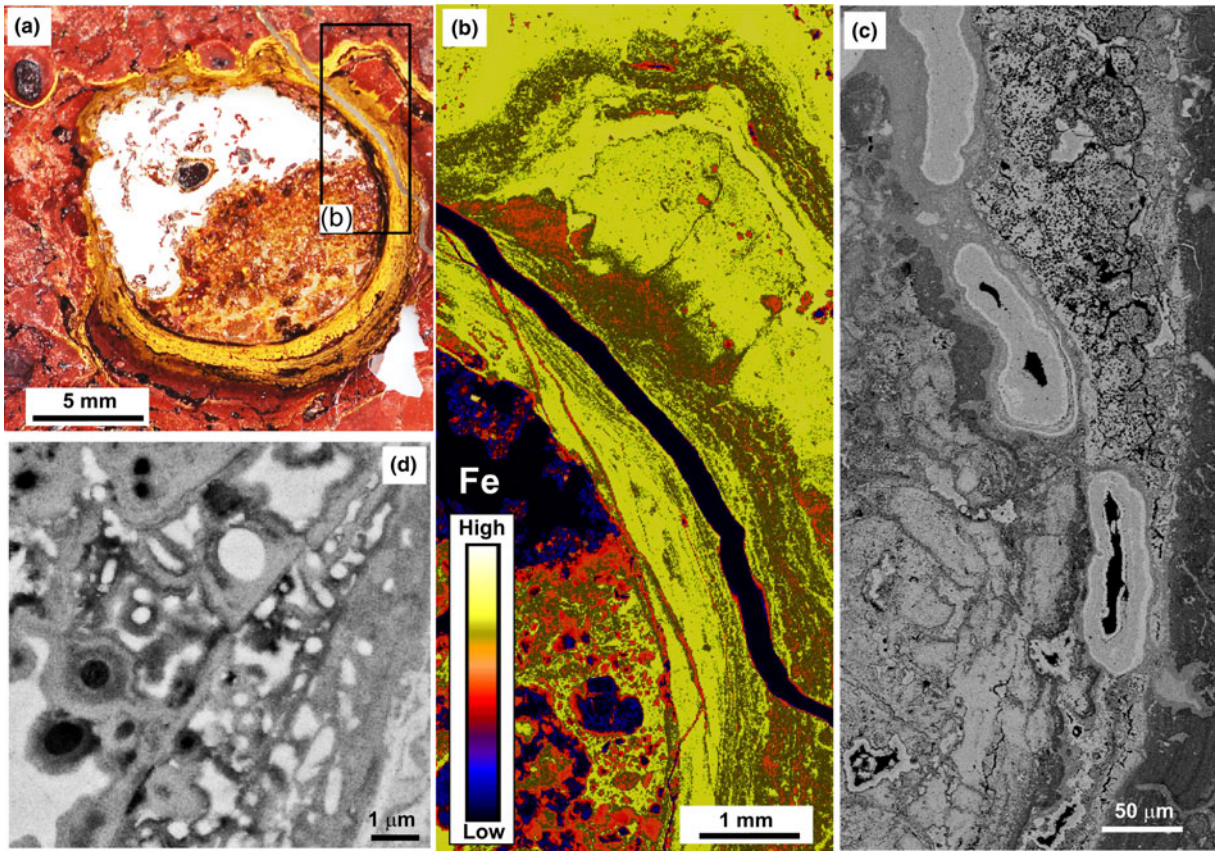

Fig. 8. Lamination in an empty root channel in canga from Serra Norte, Brazil. (a) Photograph of a horizontal cross-section with laminations inside a root channel, with (b) corresponding iron distribution from XFM. (c) Back-scattered electron image of various Fe-oxyhydroxide bands in cavities and infilling cracks. (d) Back-scattered electron image of laminations composed of per-mineralised fossils and encrusted cells enveloped by partially Al-substituted goethite.

in goethite-rich bands around root channels in our samples (Fig. 8c,d). The biogeochemical processes also mobilised and reprecipitated some aluminium as part of the microlaminated deposits in the rhizosphere (Fig. 8a–d), typically as gibbsite (e.g. Levett *et al.*, 2019).

Laminated precipitates developed during surficial gold mobility and redeposition

Laminated rims around gold particles, such as in our example from the Otago Schist terrane, New Zealand (Table 1; Fig. 9) are common in alluvial gold particles. Gold is locally mobile within supergene alteration zones and in near-surface sedimentary environments (Fig. 9a–e). Though some local Au enrichment does occur, most Au mobility results in increases in some particle sizes at the expense of other smaller particles nearby. As a consequence, gold particles can show evidence for this particle size increase as laminated rims (Fig. 9a). Supergene nuggets are commonly crystalline, and stacked layers of crystalline gold in the rim zones attest to the progressive addition of gold in the near-surface environment (Fig. 9b,c). In addition, more irregular, commonly vermiform gold overgrowths occur on both supergene nuggets, and on detrital gold particles. There is abundant evidence that gold overgrowths at the 1 to 50 µm scale have a biological component to their origins (Reith *et al.*, 2007, 2020; Kerr and Craw, 2017). The role of direct biological processes in the growth of larger nuggets is more controversial. However, biological activity such as bacterial decomposition of primary sulfide minerals in supergene zones has an indirect effect on the biogeochemical processes of Au mobility by generating metastable thiosulfate ions that can complex with Au (Shuster *et al.*, 2014).

Laminated precipitates forming manganese nodules

Manganese nodules occur on the deep ocean floor where very low sedimentation rates allow biogeochemical processes to contribute to localised metal accumulation. These nodules precipitate from metals that are mobilised from underlying abyssal sediments and metals that precipitate directly from the surrounding water, and have spectacular laminated structures (Fig. 10). Nodules have been investigated extensively as potential sources of metal resources, so geochemical, mineralogical and biological features have been well established (Hein *et al.*, 2013; Hein and Kaschinsky, 2014; Manceau *et al.*, 2014; Shiraishi *et al.*, 2016; Benites *et al.*, 2018). Here we summarise conclusions from these authors and references therein to provide a context for our general observations on the well-developed metallic laminations in our sample from the North Pacific Ocean that we depict in this paper (Fig. 10).

Manganese nodules are dominated by Mn oxides and Fe oxides, with incorporation of a range of other transition metals, particularly Cu, Co and Ni. Some primary depositional parts of the nodules undergo diagenetic transformations of mineralogy and texture, accompanied by redistribution of metals. While recent research indicates that the mobility of metals is probably linked to the structural properties of the hosting Mn oxide (Wu *et al.*, 2019), the specific minerals and metals that occur in various laminations in the

https://doi.org/10.1180/mgm.2021.8 Published online by Cambridge University Press

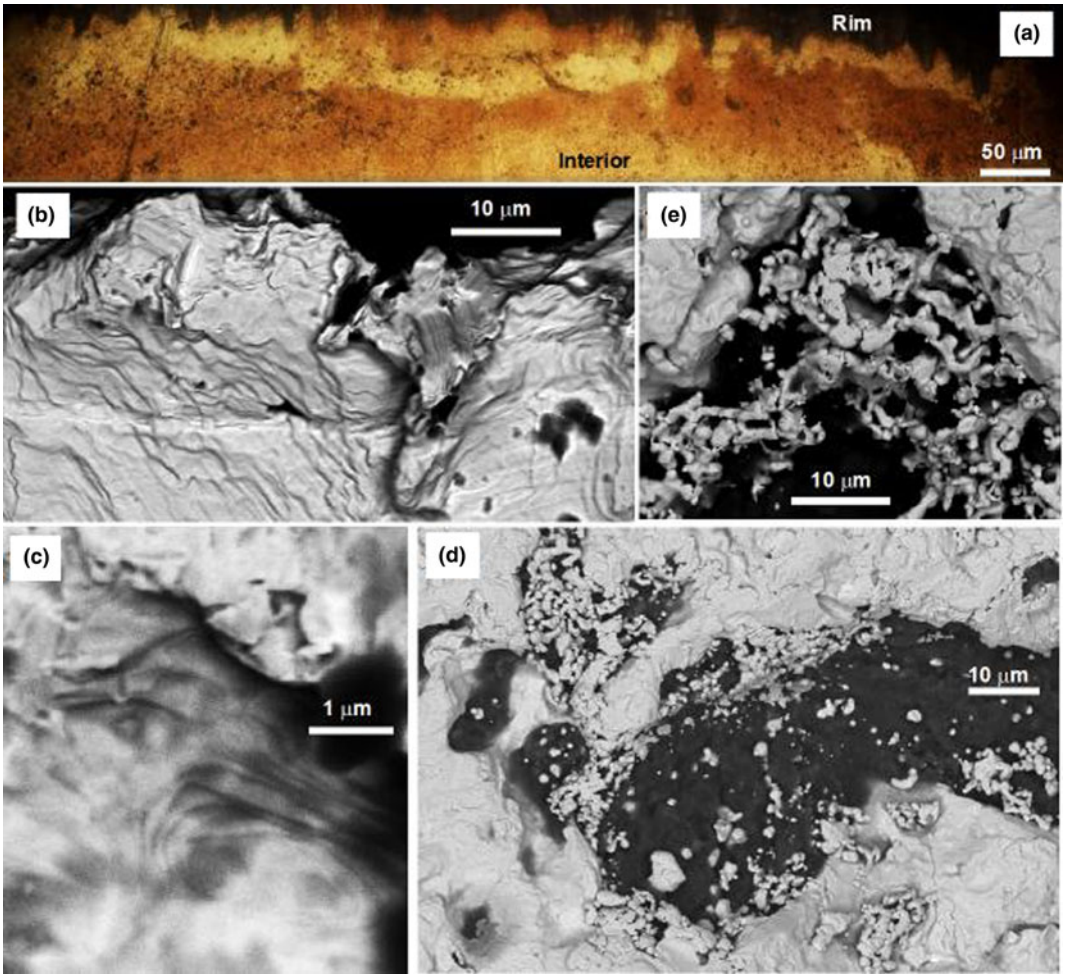

Fig. 9. Layering on the margins of gold particles from the Otago Schist terrane, New Zealand. (a) Incident light view of laminated rim of a supergene gold nugget. (b) SEM view of layered crystalline gold on the margin of a supergene nugget. (c) Magnified view of crystalline gold laminations in (b). (d) Vermiform gold overgrowths on an alluvial gold particle close to the bedrock supergene source. (e) Magnified view of vermiform gold overgrowth in (d).

nodules are also controlled by localised redox gradients that occur near to the nodule-sediment interface and the resulting diagenetic processes. Redox gradients and associated chemical activity are partially controlled by biological agents, particularly bacteria and archaea in the sediments and on the nodule surfaces. Biological processes can also facilitate localised changes in pH to more acidic conditions that differ from the ambient pH ≈ 8 of surrounding seawater. Importantly, the redox and pH gradients change with time as a result of variations in environmental factors, such as currents and changing supply of decomposing organic material. Consequently, the delicately laminated nodules record accumulation and transformation *in situ* in an environment of slow biogeochemical cycling. In our sample, there was a general separation of Mn and Fe deposition during these processes, although they were not entirely mutually exclusive (Fig. 10b,c). Likewise, other metals are generally enriched with Mn rather than Fe, but some metal-enriched Fe laminae also occur (Fig. 10b,c).

Discussion

Formation of iron-rich laminations

Iron dissolution and precipitation in surficial environments is controlled largely by reactions 4 and 5 (above). The oxygen partial pressure in many surficial environments is very low and is commonly quantified instead by redox reactions that lead to the use of Eh–pH diagrams to depict the relationships in reactions 4 and 5 (Fig. 11a). Changes in the variables in reaction 5 result in changes in the relative proportions of ferrihydrite and dissolved Fe^{2+}. Boundaries on the Eh–pH diagram (Fig. 11a) depict the combinations of the three variables in Q that lead to chemical equilibrium. The three variables in reaction 5 typically change widely in surficial environments as a result of biogeochemical processes, and disequilibrium is the norm. For example, oxidation at constant pH and $[Fe^{2+}]$ favours ferrihydrite precipitation, and reduction reverses this reaction (Fig. 11a). Conversely, acidification at constant pO_2 and $[Fe^{2+}]$ will dissolve ferrihydrite, but neutralisation will cause ferrihydrite reprecipitation (Fig. 11a).

All three variables in Q in the ferrihydrite reaction (4) are likely to change at the same time as a result of biotic and/or abiotic processes, and it is these types of fluctuations that lead to the widespread layering observed in the precipitates in our examples of laminated deposits from laboratory weathering of Cu-bearing rocks (Fig. 1), and natural samples from the supergene zones at the Salobo IOCG mine in Brazil (Figs 5, 6) and the Mt Isa mine in Australia (Fig. 7). Iron oxidation *via* reaction 4 generates hydrogen ions, and this can lead to acidification within the rocks (Singer and Stumm, 1970; Langmuir, 1997; Dockrey *et al.*, 2014). Initial

https://doi.org/10.1180/mgm.2021.8 Published online by Cambridge University Press

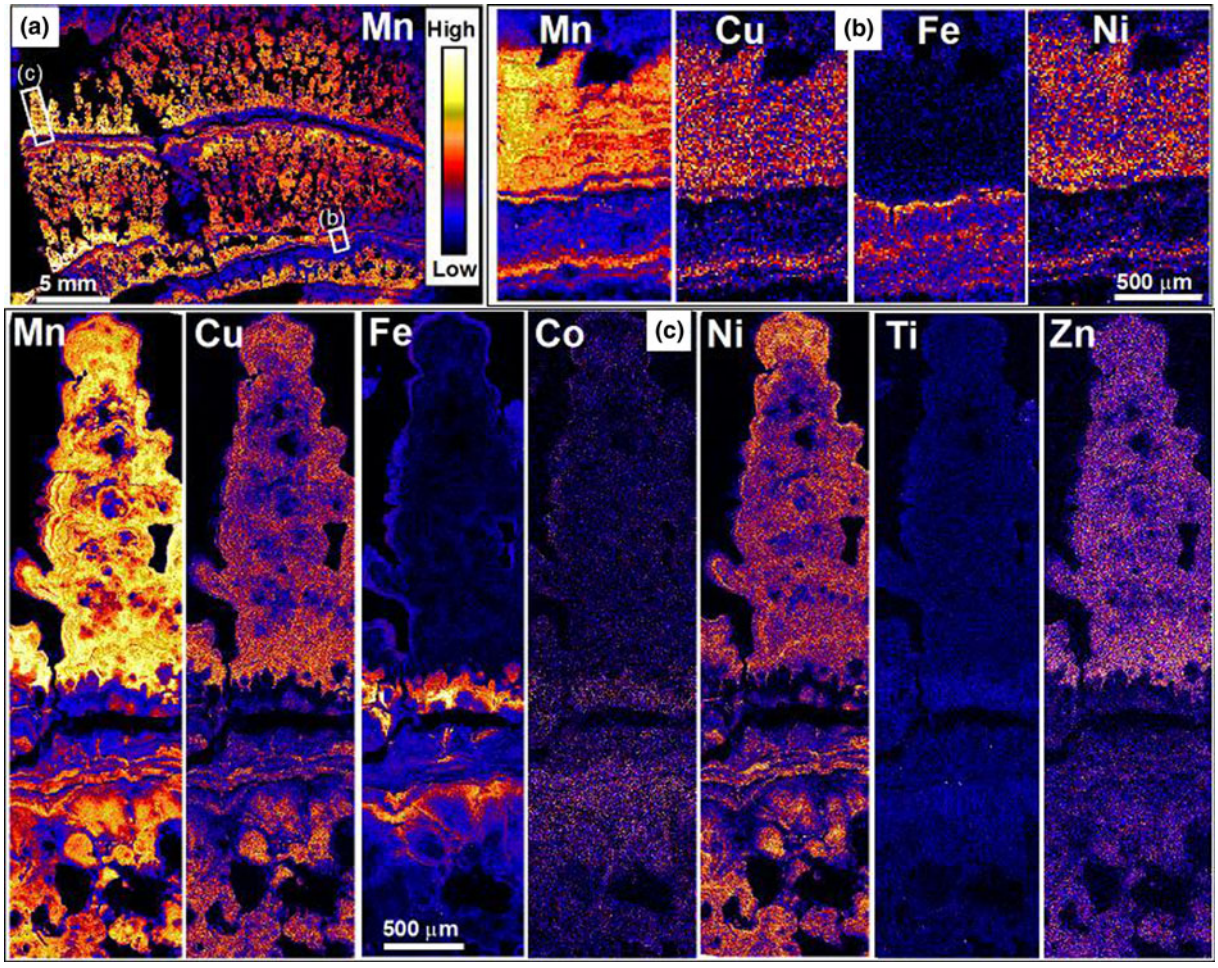

Fig. 10. XFM element-distribution maps showing laminations in a manganese nodule from the North Pacific Ocean floor. (a) General view of Mn distribution in a polished section through the nodule. (b) Magnified view of a strip through (a), showing Mn, Cu, Fe and Ni distributions in a combination of primary laminations and secondary (diagenetic) layers that truncate the primary laminae and locally obscure them. (c) XFM element-distribution maps showing a detailed view of primary metallic laminations of Mn, Cu, Fe, Co, Ni, Ti and Zn in an individual protrusion.

oxidation of ferrous to ferric iron is kinetically very slow under acidic conditions (time scales of years to centuries; Langmuir, 1997). However, bacterial mediation of the reaction can increase this rate by orders of magnitude and make it essentially instantaneous (Singer and Stumm, 1970; Langmuir, 1997; Henne *et al.*, 2019a). If the overall biogeochemical environment has a circumneutral pH and some inherent neutralising capacity, this bacterially mediated acidification may be confined to the mineral grain scale where the oxidation is focussed (Langmuir, 1997; Mielke *et al.*, 2003; Dockrey *et al.*, 2014; Henne *et al.*, 2018, 2019a,b) and result in micrometre-scale laminations at grain boundaries. Laminated precipitates in Figs 1a–e and 7e,f reflect these micrometre-scale, biologically mediated, localised variations in pH within bulk circumneutral pH. Precipitation of metal-rich laminations from the abandoned Mt Chalmers mine site in Australia depicted in Fig. 3b was driven by anthropogenic addition of neutralisation capacity with moss and algae as the substrate for precipitation. Laminations within this sample probably also reflect fluctuations in water availability linked to periods of rainfall and evaporation (Henne *et al.*, 2021), which can dilute or concentrate metals in solution and affect microbial populations that rely on water.

In our example of laminated deposits in plant root cavities at Serra Norte, Brazil (Fig. 8), organic acid production in the plant rhizosphere results in localised variations in pH and redox states in lateritic soils (Gagen *et al.*, 2019; Paz *et al.*, 2020). These biogeochemical changes, combined with associated bacterial activity, have resulted in differential Fe mobilisation and reprecipitation (Fig. 8a–d; Gagen *et al.*, 2019; Paz *et al.*, 2020; Levett *et al.*, 2020). The variable amounts of Al accompanying Fe in these laminations was mobilised as a trivalent ion and behaves in a geochemically similar manner to ferric iron and precipitates under circumneutral pH conditions (Fig. 11b). In addition, trace metals such as Co, Cr, Mn, Ti and V have been mobilised in the rhizospheric setting to form larger-scale (multiple millimetres) metal-rich laminations similar to those that occur at deeper levels (Fig. 5c), although in the surficial lateritic environment these trace metals are associated closely with Fe-oxyhydroxides (Gagen *et al.*, 2020).

In environments with less inherent neutralising capacity, bacterially mediated oxidation processes can generate larger-scale AMD (Alpers *et al.*, 2003; Lottermoser, 2010; Parbakhar-Fox and Lottermoser, 2015; Parbhakar-Fox *et al.*, 2018). At low pH, ferrihydrite is soluble, yielding dissolved Fe^{3+} under oxidising conditions (Fig. 11a,b), and this is mobile in the surficial environment until higher pH is encountered (as in Fig. 3b). The addition of abundant dissolved sulfate results in potential for precipitation of acid sulfate minerals (Fig. 11b). The laminated

https://doi.org/10.1180/mgm.2021.8 Published online by Cambridge University Press

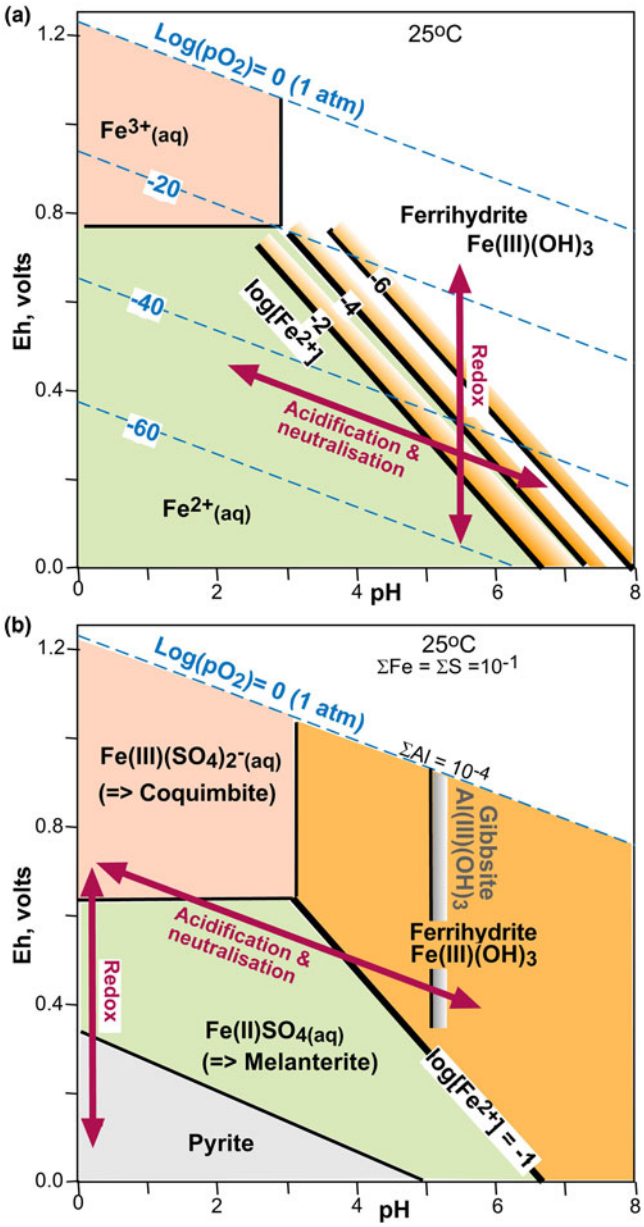

Fig. 11. Eh–pH diagrams (from *Geochemist's Workbench*, Bethke and Yeakel, 2016) showing redox relationships for Fe species in surficial environments. Heavy arrows indicate typical environmental fluctuations that lead to laminated precipitates. (a) Simple system with equilibrium lines for reaction 4 (in text) for a range of dissolved Fe^{2+}. (b) A high-sulfate system depicting fluctuations in AMD environments.

precipitates from the extreme AMD of Iron Mountain (Fig. 2e,f) result from progressive oxidation of pyrite to dissolved ferrous sulfate to dissolved ferric sulfate (cf. Fig. 11b) in a biogeochemical environment that fluctuates as a result of weather and seasonal effects on groundwater volumes, flow rates, and temperatures (Alpers *et al.*, 2003).

Laminations enriched in copper and manganese

Ferrihydrite precipitates in oxidised Cu-bearing systems almost invariably contain some Cu that has been incorporated by adsorption of dissolved Cu^{2+} (Figs 1e; 6a). This adsorption may occur when ferrihydrite precipitates during neutralisation of acid solutions generated by bacterial oxidation of ferrous iron (Fig. 12a,b). Most trace metals are immobilised readily by adsorption onto ferrihydrite. The adsorption rate is dependent on both the type of metal cation and the pH of the system (Drever, 1997; Langmuir, 1997, Henne *et al.*, 2019b). Adsorption of Cu to ferrihydrite precipitates can be enhanced by the typically large surface area of organo precipitates (Langmuir, 1997; Loiselle *et al.*, 2018) as well as by binding to functional groups (e.g. carboxyl) within such biologically mediated precipitates (Fariña *et al.*, 2018). Negatively charged cell walls of individual bacteria and associated protein structures can also form nucleation sites and lead to very localised metal accumulations as in our examples from laboratory weathering experiments (e.g. Fig. 1a–f; Konhauser, 1997). However, Cu is thermodynamically more soluble than Fe, especially under moderately acidic to alkaline conditions (Fig. 12a–c). Therefore, Cu can be more mobile and form separate precipitates in many surficial environments at a range of spatial scales, such as in our examples from surface discharge at the Mt Chalmers mine, the supergene zone at the Salobo IOCG mine, and our example of a manganese nodule from the ocean floor (Figs 3; 5; 10). Manganese has similar solubility to Cu under oxidised surficial conditions, so Cu and Mn can readily precipitate, either together, or in close proximity. Subtle biogeochemical fluctuations under circumneutral pH conditions, where Cu and Mn solubility boundaries have slightly different slopes (Fig. 12a), can apparently result in laminae with differing Cu and Mn contents at the 10 µm scale as seen in the supergene zone at Salobo and our manganese nodule example (Figs 5c; 10).

Laminae with minerals of differing Cu oxidation states were examined in samples from the supergene zone at Salobo and reflect the progressive incursion of oxygen into more reduced settings, causing oxidation of the Cu and transformation of the mineralogy (Fig. 12b). Hence, boundaries between these mineral laminae are dynamic features that migrate progressively into more reduced environments, yielding laminated redox gradients on the millimetre scale or less (e.g. Figs 6b; 7c–f). It is also notable that in some surficial environments (e.g. the surface discharge at Mt Chalmers and the supergene zone at Mt Isa), there has been negligible incorporation of Mn within Cu precipitates (Figs 3b; 7), at least partly because Mn is more soluble than Cu under less-oxidised circumneutral pH conditions within such a redox gradient (Fig. 12a).

Minor incorporation of other transition metals into laminated metallic precipitates occurs principally in Cu- and Mn-rich laminae rather than Fe-rich laminae, reflecting the similar solubility of these minor metals to Cu and Mn under oxidised conditions. For example, co-precipitation of Zn with Cu is pronounced under the circumneutral conditions of neutralised AMD at Mt Chalmers (Fig. 3b; 12c). Similarly, Zn and Ni, and to a lesser extent Co, principally follow Cu and Mn during laminated manganese nodule formation, whereas greater Ti enrichment accompanies Fe deposition (Fig. 10b,c). However, Ti and V also accompany Cu and Mn in the subaerial weathering profile at Salobo (Fig. 5c) and some organisms (e.g. algae) are known for their metal-specific biosorption capacity (via ion exchange, complex formation and electrostatic interaction; Mata *et al.*, 2008; Demirbas, 2008; Zeraatkar *et al.*, 2016), which can further influence metal concentrations in laminae (e.g. a potential process in discharging waters at Mt Chalmers; Fig. 3).

Laminated precipitates related to gold deposits

Metalloids Sb and As are typically abundant around orogenic gold deposits (Craw and Kerr, 2017). Both these metalloids are variably

https://doi.org/10.1180/mgm.2021.8 Published online by Cambridge University Press

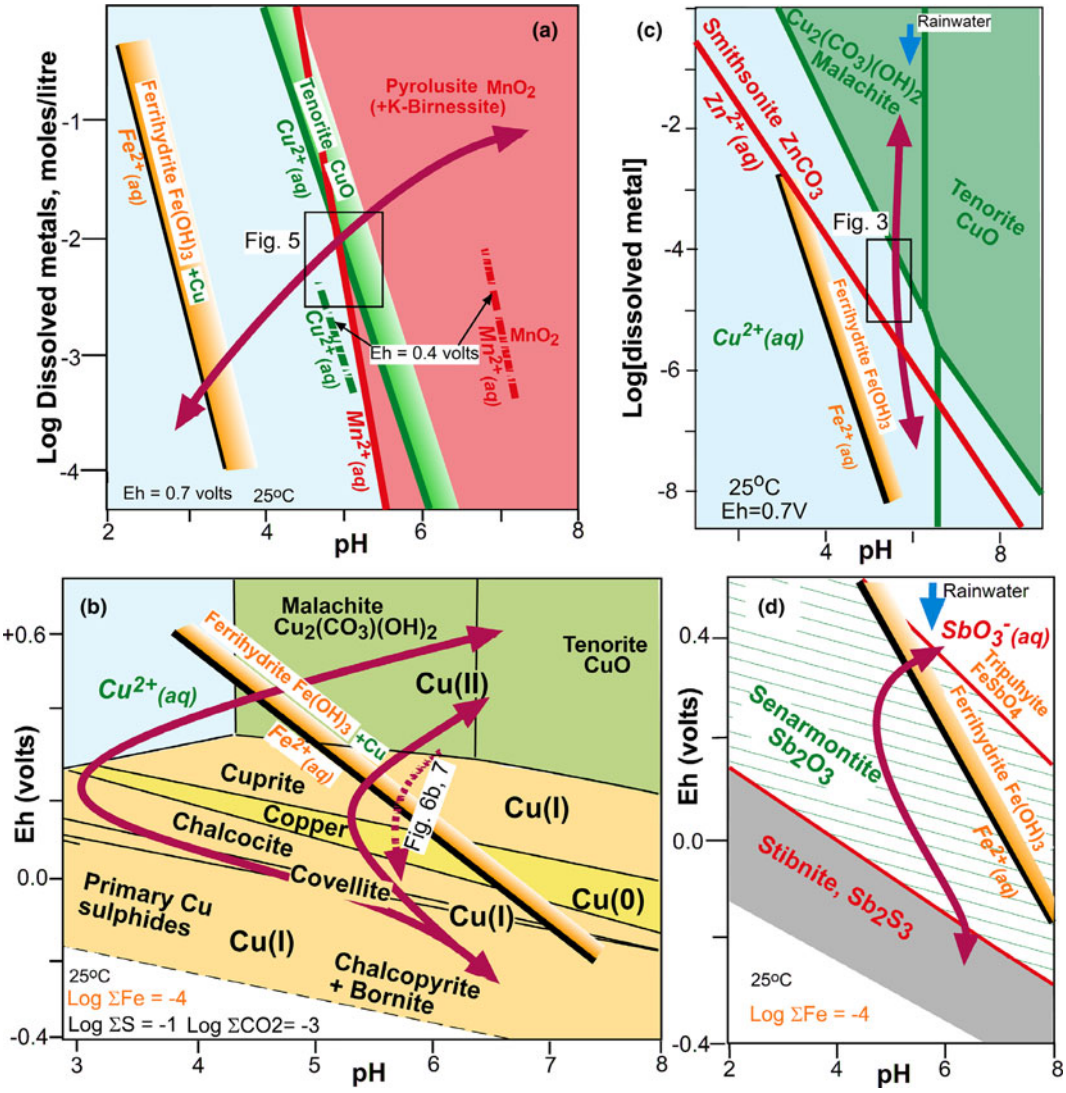

Fig. 12. Geochemical models (from *Geochemist's Workbench*) showing relationships between dissolved metals and precipitates. Heavy arrows indicate typical environmental variations across equilibrium boundaries that lead to laminated precipitates. (a) Comparisons of solubility of Cu with Fe and Mn in oxidised environments (Eh = 0.7 V). Relative solubilities of Cu and Mn under more reducing conditions (Eh = 0.4 V) are indicated. (b) Eh–pH diagram for Cu. (c) Comparison of solubility of Cu with Zn and Fe in oxidised environments (Eh = 0.7 V). (d) Eh–pH diagram for Sb (for example in Fig. 4a–d).

soluble in the surficial environment and they are especially susceptible to variations in redox and pH conditions (Figs 12d; 13a). In both examples outlined in this paper (the Au–As–Sb orogenic deposit in Otago and the Waiuta orogenic gold mine), there is evidence for a wide range of redox conditions, from reduced sulfides to fully oxidised precipitates at sub-millimetre scales (Figs 2a,b; 4a–d). There is also textural evidence for biogeochemical fluctuations leading to complex mineralogical layering within these redox gradients (Figs 2a,b; 4a–d).

The redox gradient developed on stibnite (Fig. 4a–d) is a result of similar weathering-driven progressive oxygen incursion to that observed on the native copper sample from Mt Isa (Fig. 7c–f). However, because of the young age and incipient nature of the weathering of the stibnite deposit, a more complete redox gradient has developed on a narrow spatial scale (Fig. 4a–d). Seasonal variations in rainfall and temperature undoubtedly had an effect on the biological effects on sulfide oxidation in the deposit, and also the effectiveness of physical incursion of oxidised rainwater. Localised bacterially mediated acidification from sulfide oxidation within the oxidising rock mass was countered by incursion of circumneutral rainwater and calcite in adjacent rocks during oxidation (Fig. 12d). The exact stability boundaries of tripuhyite are not known, but it is the most oxidised Sb–Fe mineral in this system coexisting with ferrihydrite (Fig. 4a; 12d). In contrast, textures of secondary stibnite (Fig. 4a–d) suggest that biologically mediated reduction of Sb and S has also occurred at times. Senarmontite crystals (Fig. 4a–c) attest to precipitation under intermediate redox stages that may have occurred during both oxidation and reduction (Fig. 12d).

Our As-bearing example from the Au–As–Sb orogenic sample (Fig. 2a,b; Table 1) also shows evidence for complex layering of both oxidation and reduction precipitates within the broad redox gradient defined by Fe(III)–As(V)-oxyhydroxide precipitates (Fig. 2a) that probably include ferrihydrite and scorodite (Fig. 13a) and the authigenic sulfide mineral realgar (Figs 2a,b; 13a). Arsenolite is an extremely soluble As mineral but dissolved

https://doi.org/10.1180/mgm.2021.8 Published online by Cambridge University Press

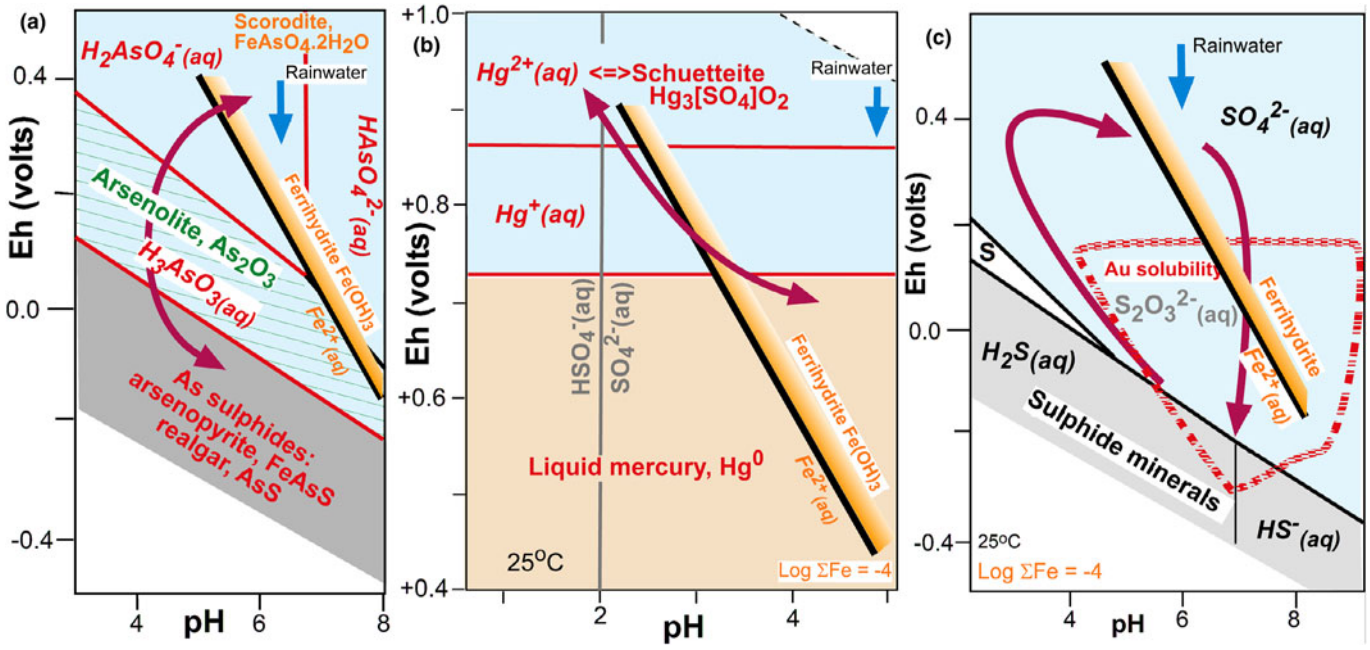

Fig. 13. Eh–pH diagrams (from *Geochemist's Workbench*) showing redox relationships for: (a) As (for example in Fig. 2a,b); (b) Hg (for example in Fig. 2c,d); and (c) Au (for example in Fig. 9). Heavy arrows indicate typical environmental variations across equilibrium boundaries that lead to laminated precipitates.

As concentrations in this deposit reach very high levels, facilitating precipitation under intermediate redox conditions (Fig. 13a; Haffert *et al.*, 2010; Andrade *et al.*, 2010), possibly during both oxidation and reduction stages. The most reduced end of the redox gradient is maintained by decomposing organic material. Dissolution of scorodite causes localised acidification, while incursion of oxygenated rainwater during frequent major rain events in the area can change pH and Eh (Fig. 13a; Davies *et al.*, 2011; Kerr *et al.*, 2018).

Mercury redistribution and associated laminations with varying Hg contents in the Waiuta sample (Fig. 2c,d) are caused by similar biochemical variations to As and Sb (Fig. 13b). In our dry-climate mine tailings example (Table 1), the deposit is highly oxidised and acidic because of biologically mediated sulfide oxidation that is on-going. Consequently, remnants of liquid Hg that were added to the tailings have generally been oxidised to schuetteite (Fig. 2c,d; 13b). However, carbonaceous material and relict sulfides in the deposit appear to cause local reduction and, locally, re-reduction of schuetteite to liquid Hg has occurred. (Fig. 2d; 13b).

Gold is mobile in the surficial environment where incipient oxidation of sulfide minerals yields metastable thiosulfate ions ($S_2O_3^{2-}$) that provide ligands for Au solubility at circumneutral pH (Fig. 13c; Webster, 1986; Lengke and Southam, 2007). Decomposition of the thiosulfate ions over time, after further oxidation, and/or any acidification, results in gold deposition. In addition, gold can be mobilised with HS^- ions as ligands under relatively reduced conditions in a narrow circumneutral pH band (Fig. 13c; Webster, 1986). Hence, in a dynamic biogeochemical environment, gold can be dissolved and re-precipitated as a result of variations in pH, redox state, or both. In particular, bacterially mediated sulfide oxidation provides ideal biogeochemical gradients for gold redistribution (Fig. 13c; Reith *et al.*, 2006, 2007, 2013; Lengke and Southam, 2007; Johnston *et al.*, 2013; Shuster *et al.*, 2016). Biogeochemical cycling that involves sulfide oxidation and episodic rainwater or groundwater incursion is therefore likely to result in laminated gold deposition and additions of authigenic gold to pre-existing gold particles (e.g. the Otago Schist sample pictured in Fig. 9a–d; 13c; Reith *et al.*, 2006, 2007, 2012a, 2013, 2020).

Conclusions and implications

The mobility and (re)precipitation of metals in near-surface environments is driven primarily by geochemical disequilibrium, especially with respect to pH and redox states. Gradients in pH and redox conditions in rocks and associated shallow groundwaters develop on a range of spatial and temporal scales. These gradients are formed from, and subsequently affected by, complex interactions between biological and geological processes. Hence, different degrees of chemical disequilibrium arise on vast spatial (microenvironments to planetary) and temporal scales (days to millennia). Metalliferous mineral deposition results from subsequent supersaturation of waters that arise as a result of disequilibrium at the prevailing geochemical conditions. Changing conditions result in deposition of different minerals that reflect different degrees of supersaturation, leading to the formation of fine-scale laminations of metalliferous deposits.

In our examples, the biological component of these small near-surface settings with enhanced metal mobility is dominated by chemolithotrophic bacteria, such as Fe- and S-oxidisers and/or reducers. However, other entities such as archaea, algae, plants, mosses, fungi and microinvertebrates can also affect the biogeochemistry of natural systems. Sulfur- and Fe-oxidising bacteria are common chemolithotrophs that affect sulfide-bearing metal deposits because of the influence of nearby air and oxygenated shallow groundwater. However, localised reductive environments can develop around decaying organic material and/or partially decomposed sulfide minerals, thereby, enabling reducing bacteria to play a role in the development of complex redox gradients in such settings. Biological entities that are not actively oxidising or reducing metals, can be relatively passive occupants of these metalliferous environments, and merely provide substrates with large surface area for

https://doi.org/10.1180/mgm.2021.8 Published online by Cambridge University Press

deposition of precipitates. Bacteria can also take passive advantage of on-going mineral reactions driven by geochemical disequilibrium and can contribute to those reactions by catalysing the kinetic reaction rates. In doing so, the metabolic processes of bacteria can cause localised changes to the biogeochemical environments, especially with respect to pH and redox conditions that can lead to metal dissolution and/or metal deposition.

The laminated metalliferous deposits outlined in this paper have complex biogeochemical parageneses, which are not predictable because there are many varied parameters that affect their respective formation. However, some generalisations can be made. For example, there is commonly a spatial separation of Fe-rich precipitates from those with Cu and Mn because of the greater solubility of the latter metals under weakly acidic and oxidised conditions. Other transition metals such as Ni, V and Zn also follow Cu and Mn rather than Fe. In contrast, metalloids As and Sb have a strong affinity for Fe under oxidising conditions, but not under more reduced conditions. There is, however, inevitably some overlap between these general trends.

The laminated deposits described in this paper are small, but they reflect the types of biogeochemical processes that can pervade all near-surface environments. The textures, mineral species, and metal associations within these deposits are likely to be encountered in all facets of mineral deposit development: initial exploration activity of near-surface locations; mining of shallow portions of orebodies, especially supergene zones; and in downstream environmental issues with respect to discharging metalliferous waters.

Acknowledgements. Parts of this research were funded by the Australian Research Council Linkage Programs LP140100804 and LP140100805, and parts were supported by the Royal Society of New Zealand via the Marsden Fund. Many of the images and associated data were obtained from the XFM beamline at the Australian Synchrotron, part of ANSTO, in Melbourne, Australia. Some SEM work was carried out at the Centre for Microscopy and Microanalysis at the University of Queensland, where we thank Ron Rasch and Kim Sewell for their excellent support. Additional SEM work was carried out at Otago Micro and Nanoscale Imaging (OMNI), University of Otago, with able assistance of Kat Lilley. Field work to collect rocks and bacterial ecosystems in Brazil was supported by the mining staff from the Vale Salobo mine. Field work to collect bacterial ecosystems from Mount Chalmers in Queensland was funded and supported by the Department of Natural Resources, Mines and Energy in Queensland. Manganese nodule samples were supplied by Simon Richards from Adrok Ltd.

References

Alpers C.N., Nordstrom D.K. and Spitzley J. (2003) Extreme acid mine drainage from a pyritic massive sulfide deposit, the Iron Mountain end-member. Pp 407–430 in: *Environmental Aspects of Mine Wastes* (J.L. Jambor, D.W. Blowes and A.I.M. Ritchies, editors). Mineralogical Association of Canada, Ottawa.

Andrade C.F., Jamieson H.E., Kyser T.K., Praharaj T. and Fortin, D. (2010) Biogeochemical redox cycling of arsenic in mine-impacted lake sediments and co-existing pore waters near Giant Mine, Yellowknife Bay, Canada. *Applied Geochemistry*, **25**, 199–211.

Baker B.J. and Banfield J.F. (2003) Microbial communities in acid mine drainage. *FEMS. Microbiology Ecology*, **44**, 139–152.

Benites M., Millo C., Hein J., Nath B.N., Murton B., Galante D. and Jovane, L. (2018) Integrated geochemical and morphological data provide insights into the genesis of ferromanganese nodules. *Minerals*, **8**, 488, https://doi.org/10.3390/min8110488

Bethke C.M. and S. Yeakel (2016) *The Geochemist's Workbench®, Release 11: GWB Essentials Guide*. Aqueous Solutions LLC, Champaign, Illinois, USA, 151 pp.

Craw D. and Lilly K. (2016) Gold nugget morphology and geochemical environments of nugget formation, southern New Zealand. *Ore Geology Reviews*, **79**, 301–315.

Craw D. and Kerr G. (2017) Geochemistry and mineralogy of contrasting supergene gold alteration zones, southern New Zealand. *Applied Geochemistry*, **85**, 19–34.

Craw D., MacKenzie D.J. and Grieve P. (2015) Supergene gold mobility in orogenic gold deposits, Otago Schist, New Zealand. *New Zealand Journal of Geology and Geophysics*, **58**, 123–136.

Davies, H., Weber, P., Lindsay, P., Craw, D. and Pope, J., 2011. Characterisation of acid mine drainage in a high rainfall mountain environment, New Zealand. *Science of the Total Environment*, **409**, 2971–2980.

Deamer D. and Weber A.L. (2010) Bioenergetics and Life's Origins. *Cold Spring Harb Perspect Biology*, **2**, a004929, https://doi.org/10.1101/cshperspect.a004929

Demirbas A. (2008) Heavy metal adsorption onto agro-based waste materials: a review. *Journal of Hazardous Materials*, **157**, 220–229.

Dockrey J., Lindsay M., Mayer K., Beckie R., Norlund K., Warren L. and Southam G. (2014) Acidic microenvironments in waste rock characterized by neutral drainage: Bacteria–mineral interactions at sulphide surfaces. *Minerals*, **4**, 170–190.

Dold B. (2014) Evolution of acid mine drainage formation in sulphidic mine tailings. *Minerals*, **4**, 621–641.

Drever J.I. (1997) *The Geochemistry of Natural Water: Surface and Groundwater Environments*. 3rd Edition, Prentice Hall, New Jersey, USA.

Enders M.S., Knickerbocker C., Titley S.R. and Southam G. (2006) The role of bacteria in the supergene environment of the Morenci porphyry copper deposit, Greenlee County, Arizona. *Economic Geology*, **101**, 59–70.

Fariña A.O., Peacock C.L., Fiol S., Antelo J. and Carvin B. (2018) A universal adsorption behaviour for Cu uptake by iron (hydr)oxide organo-mineral composites. *Chemical Geology*, **479**, 22–35.

Gadd G.M. (2007) Geomycology: biogeochemical transformations of rocks, minerals, metals and radionuclides by fungi, bioweathering and bioremediation. *Mycology Research*, **111**, 3–49.

Gadd G.M. (2010) Metals, minerals and microbes: geomicrobiology and bioremediation. *Microbiology*, **156**, 609–643.

Gagen E.J., Levett A., Paz A., Gastauer M., Caldeira C.F., Valadares R.B.S., Bitencourt J.A.P., Alves R., Oliveira G., Siqueira J.O., Vasconcelos P.M. and Southam G. (2019). Biogeochemical processes in canga ecosystems: Armoring of iron ore against erosion and importance in iron duricrust restoration in Brazil. *Ore Geology Reviews*, **107**, 573–586.

Haffert L., Sander S.G., Hunter K.A. and Craw D. (2010) Evidence for arsenic-driven redox chemistry in a wetland system: A field voltammetric study. *Environmental Chemistry*, **7**, 386–397.

Heim, C. (2011) Microbial biomineralization. In: *Encyclopedia of Geobiology* (J. Reitner, V. Thiel, editors). Geobiology Group Geoscience Centre, University of Göttingen, Göttingen, Germany.

Hein J.R. and Koschinsky A. (2014). *Deep-ocean ferromanganese crusts and nodules*. Pp. 273–291 in: *Geochemistry of Mineral Deposits*. Treatise on Geochemistry, 2nd Ed, Vol 13. Elsevier, The Netherlands.

Hein J.R., Mizell K., Koschinsky A. and Conrad T.A. (2013) Deep-ocean mineral deposits as a source of critical metals for high- and green-technology applications: Comparison with land-based resources. *Ore Geology Reviews*, **51**, 1–14.

Henne A., Craw D., Vasconcelos P. and Southam G. (2018) Bioleaching of waste material from the Salobo mine, Brazil: Recovery of refractory copper from Cu hosted in silicate minerals. *Chemical Geology*, **498**, 72–82.

Henne A., Craw D., Gagen E.J. and Southam, G. (2019a) Bacterially-mediated supergene alteration and redistribution of copper in mineralised rocks at the Salobo IOCG deposit, Brazil. *Ore Geology Reviews*, **115**, 103210.

Henne A., Craw D., Gagen E.J. and Southam G. (2019b) Bacterial influence on storage and mobilisation of metals in iron-rich mine tailings from the Salobo mine, Brazil. *Science of the Total Environment*, **680**, 91–104.

Henne A., Craw D., Gagen E.J. and Southam G. (2020) Contribution of bacterially-induced oxidation of Fe-silicates in iron-rich ore to laterite formation, Salobo IOCG mine, Brazil. *Chemical Geology*, **539**, https://doi.org/10.1016/j.chemgeo.2020.119499

https://doi.org/10.1180/mgm.2021.8 Published online by Cambridge University Press

Henne A., Craw D., Gagen E.J. and Southam G. (2021) Metalliferous biofilm formation in low-Fe waters at the sulphidic Mount Chalmers mine, Queensland, Australia. Unpublished data.

Johnson D.B. and Hallberg K.B. (2005) Acid mine drainage remediation options: A review. *Science of the Total Environment*, **338**, 3–14.

Johnston C.W., Wyatt M.A., Li X., Ibrahim A., Shuster J., Southam G. and Magarvey N. (2013) Gold biomineralization by a metallophore from a gold-associated microbe. *Nature Chemical Biology*, **9**, 241–243.

Kerr G. and Craw D. (2017) Mineralogy and geochemistry of biologically mediated gold mobilisation and redeposition in a semiarid climate, southern New Zealand. *Minerals*, **7**, 147, https://doi.org/10.3390/min7080147

Kerr G. and Craw, D. (2020) Metal redistribution during cementation of historic processing residues, Macraes gold mine, New Zealand. *New Zealand Journal of Geology and Geophysics*, **63**, https://doi.org/10.1080/00288306.2020.1787472

Kerr G., Craw D., Pope J. and Trumm D. (2018) Authigenic realgar and gold in dynamic redox gradients developed on historic mine wastes, New Zealand. *Applied Geochemistry*, **97**, 123–133.

Konhauser K.O. (1997) Bacterial iron biomineralisation in nature. *FEMS Microbiology Reviews*, **20**, 315–326.

Langmuir D. (1997) *Aqueous Environmental Geochemistry*. Prentice Hall, Upper Saddle River New Jersey, USA.

Lengke M. and Southam G. (2007) The deposition of elemental gold from gold (I) thiosulfate complexes mediated by sulfate-reducing bacterial conditions. *Economic Geology*, **102**, 109–126.

Levett A., Gagen E.J., Diao H., Guagliardo P., Rintoul L., Paz A., Vasconcelos P.M. and Southam G. (2019) The role of aluminium in the preservation of microbial biosignatures. *Geoscience Frontiers*, **10**, 1125–1138.

Levett A., Vasconcelos P.M., Gagen E.J., Rintoul L., Spier C., Guagliardo P. and Southam G. (2020) Microbial weathering signatures in lateritic ferruginous duricrusts. *Earth and Planetary Science Letters*, **538**, 116209.

Loiselle L., McCraig M.A., Dyar M.D., Léveillé R., Shieh S.R. and Southam G. (2018) A spectral comparison of jarosites using techniques relevant to the robotic exploration of biosignatures on Mars. *Life*, **8**, 61.

Lottermoser B. (2010) *Mine Wastes: Characterization, Treatment and Environmental Impacts*. Springer, Berlin, 400 pp.

Manceau A., Lanson M. and Takahashi Y. (2014) Mineralogy and crystal chemistry of Mn, Fe, Co, Ni, and Cu in a deep-sea Pacific polymetallic nodule. *American Mineralogist*, **99**, 2068–2083.

Mata Y.N., Blazquez M.L., Ballester A., Gonzalez F. and Munoz J.A. (2008) Characterization of the biosorption of cadmium, lead and copper with the brown alga Fucus vesiculosus. *Journal of Hazardous Materials*, **158**, 316–323.

Mielke R.E., Pace D.L., Porter T. and Southam G. (2003) A critical stage in the formation of acid mine drainage: Colonization of pyrite by *Acidithiobacillus ferrooxidans* under pH-neutral conditions. *Geobiology*, **1**, 81–90.

Nordstrom D.K., and Southam, G. (1997) Geomicrobiology of sulfide mineral oxidation. Pp. 361–390 in: *Geomicrobiology: Interactions between Microbes and Minerals* (J.F. Banfield and K.H. Nealson, editors). Reviews in Mineralogy, **35**. Mineralogical Society of America, Chantilly, Virginia, USA.

Parbhakar-Fox A. and Lottermoser B.G. (2015) A critical review of acid rock drainage prediction methods and practices. *Minererals Engineering*, **82**, 107–124.

Parbhakar-Fox A., Fox N., Jackson L. and Cornelius R. (2018) Forecasting geoenvironmental risks: Integrated applications of mineralogical and chemical data. *Minerals*, **8**, 541–562.

Paterson D., de Jonge M.D., Howard D.L., Lewis W., McKinlay J., Starritt A., Kusel M., Ryan C.G., Kirkham R., Moorhead G. and Siddons D.P. (2011) The X-ray fluorescence microscopy beamline at the Australian synchrotron. *AIP Conference Proceedings*, **1365**, 219–222.

Paz A., Gagen E.J., Levett A., Zhao Y., Kopittke P.M. and Southam G. (2020) Biogeochemical cycling of iron oxides in the rhizosphere of plants grown on ferruginous duricrust (canga). *Science of the Total Environment*, **713**, 136637.

Pope J.G., McConchie D.M., Clark M.D. and Brown K.L. (2003) Diurnal variations in the chemistry of geothermal fluids after discharge, Champagne Pool, Waiotapu, New Zealand. *Chemical Geology*, **203**, 253–272.

Quatrini R. and Johnson D.B. (2018) Microbiomes in extremely acidic environments: functionalities and interactions that allow survival and growth of prokaryotes at low pH. *Current Opinion in Microbiology*, **43**, 139–147.

Ravel B. and Newville M. (2005) ATHENA, ARTEMIS, HEPHAESTUS: data analysis for X-ray absorption spectroscopy using IFEFFIT. *Journal of Synchrotron Radiation*, **12**, 537–541.

Reith F., Rogers S.L., McPhail D.C. and Webb D. (2006) Biomineralization of gold: biofilms on bacterioform gold. *Science*, **313**, 233–236.

Reith F., Lengke M.F., Falconer D., Craw, D. and Southam, G. (2007) The geomicrobiology of Au: *International Society for Microbial Ecology Journal*, **1**, 567–584.

Reith F., Brugger J., Zammit C.M., Gregg A.L., Goldfarb K.C., Andersen G.L., DeSantis T.Z., Piceno Y.M., Brodie E.L. and Lu Z. (2012a) Influence of geogenic factors on microbial communities in metallogenic Australian soils. *International Society for Microbial Ecology*. **6**, 2107–2118.

Reith F., Stewart L. and Wakelin S.A. (2012b). Supergene gold transformation: secondary and nano-particulate gold from Southern New Zealand. *Chemical Geology*, **320**, 32–45.

Reith F., Brugger J., Zammit C.M., Nies D.H. and Southam G. (2013). Geobiological cycling of gold: From fundamental process understanding to exploration solutions. *Minerals*, **3**, 367–394.

Reith F., Zammit C.M., Pohrib R., Gregg A.L. and Wakelin S.A. (2015). Geogenic factors as drivers of microbial community diversity in soils overlying polymetallic deposits. *Applied and Environmental Microbiology*, **81**, 7822–7832.

Reith F., Falconer D.M., Van Nostrand J., Craw D., Shuster J. and Wakelin S. (2020) Functional capabilities of bacterial biofilms on gold particles. *FEMS Microbiology and Ecology*, **96**, https://doi.org/10.1093/femsec/fiz196

Ryan C.G. (1999) *GeoPIXE software for PIXE and SXRF imaging*. Available at http://nmp.csiro.au/GeoPIXE.html

Ryan C.G., Siddons D.P., Kirkham R., Dunn P.A., Kuczewski A., Moorhead G., De Geronimo G., Paterson D.J., de Jonge M.D., Hough R.M., Lintern M.J., Howard, D.L., Kappeng P. and Cleverleya J. (2010) The new Maia detector system: Methods for high definition trace element imaging of natural material. *AIP Conference Proceedings*, **1221**, 9.

Ryan C.G., Siddons D.P., Kirkham R., Li, Z.Y., de Jonge M.D., Paterson D.J., Kuczewski A., Howard D.L., Dunn P.A., Falkenberg G., Boesenberg U., De Geronimo G., Fisher L.A., Halfpenny A., Lintern M.J., Lombi E., Dyl K.A., Jensen M., Moorhead G.F., Cleverley J.S., Hough R.M., Godel B., Barnes S.J., James S.A., Spiers K.M., Alfeld M., Wellenreuther G., Vukmanovic Z. and Borg S. (2014) Maia X-ray fluorescence imaging: Capturing detail in complex natural samples. *Journal of Physics: Conference Series*, **499**, 012002–13.

Salama W., Gazley M.F. and Bonnett L.C. (2016) Geochemical exploration for supergene copper oxide deposits, Mount Isa Inlier, NW Queensland, Australia. *Journal of Geochemical Exploration*, **168**, 72–102.

Sanyal S.K., Shuster J. and Reith F. (2019) Cycling of biogenic elements drives biogeochemical gold cycling. *Earth-Science Reviews*, **190**, 131–147.

Shiraishi F., Mitsunobu S., Suzuki K., Hoshino T., Morono Y. and Inagaki F. (2016) Dense microbial community on a ferromanganese nodule from the ultra-oligotrophic South Pacific Gyre: Implications for biogeochemical cycles. *Earth and Planetary Science Letters*, **447**, 10–20.

Shuster J., Bolin T., MacLean L.C.W. and Southam G. (2014) The effect of iron-oxidising bacteria on the stability of gold (I) thiosulphate complex. *Chemical Geology*, **376**, 52–60.

Shuster J., Lengke M., Marquez-Zavalia M.F. and Southam G. (2016) Floating gold grains and nanophase particles produced from the biogeochemical weathering of a gold-bearing ore. *Economic Geology*, **111**, 1485–1494.

Shuster J., Reith F., Izawa M.R.M., Flemming R.L., Banerjee N.R. and Southam G. (2017) Biogeochemical cycling of silver in acidic, weathering environments. *Minerals*, **7**, 218.

Shuster J., Rea M.A., Etschmann B., Brugger J. and Reith F. (2018) Terraced iron formations: Biogeochemical processes contributing to microbial biomineralization and microfossil preservation. *Geosciences*, **8**, 480.

Singer P.C. and Stumm W. (1970) Acid mine drainage: The rate-determining step. *Science*, **167**, 1121–1123.

Wakelin S.A., Anand R.R., Reith F., Gregg A.L., Noble R.R.P. and Goldfarb K.C. (2012a) Bacterial communities associated with a mineral weathering profile at a sulphidic mine tailings dump in arid Western Australia. *FEMS Microbiology Ecology*, **79**, 298–311.

https://doi.org/10.1180/mgm.2021.8 Published online by Cambridge University Press

Wakelin S.A., Anand R.R., Reith F., Macfarlane C. and Rogers S. (2012b) Biogeochemical surface expression over a deep, overburden-covered VMS mineralization. *Journal of Geochemical Exploration*, **112**, 262–271.

Warren L.A. and Haack E.A. (2001) Biogeochemical controls on metal behaviour in freshwater environments. *Earth Science Reviews*, **54**, 261–320.

Webster J.G. (1986) The solubility of Au and Ag in the system Au-Ag-S-O_2-H_2O at 25°C and 1 atm. *Geochimica et Cosmochimica Acta*, **50**, 245–255.

Wu Z., Peacock C.L., Lanson B., Yin H., Zheng L., Chen Z., Tan W., Qiu G., Liu F. and Feng X. (2019) Transformation of Co-containing birnessite to todorokite: Effect of Co on the transformation and implications for Co mobility. *Geochimica et Cosmochimica Acta*, **246**, 21–40.

Zeraatkar A.K., Ahmadzadeh H., Talebi A.F., Moheimani N.R. and McHenry M.P. (2016) Potential use of algae for heavy metal bioremediation, a critical review. *Journal of Environmental Management*, **181**, 817–831.

https://doi.org/10.1180/mgm.2021.8 Published online by Cambridge University Press